International Journal Of Greenhouse Gas Control
May 2015, Volume 36 Pages 78-92
https://doi.org/10.1016/j.ijggc.2015.02.018
https://archimer.ifremer.fr/doc/00692/80388/

Phase behavior of (CO2 + H-2) and (CO2+ N-2) at temperatures between (218.15 and 303.15)K at pressures up to 15 MPa

Fandino Olivia [1], Trusler J. P. Martin [1,*], Vega-Maza David [1]

[1] Univ London Imperial Coll Sci Technol & Med, Dept Chem Engn, London SW7 2AZ, England.

* Corresponding author : Trusler J. P. Martin, email address : m.trusler@imperial.ac.uk

Abstract :

Vapor-liquid equilibrium data are reported for the binary systems (CO2+H-2) and (CO2 +N-2) at temperatures between (218.15 and 303.15)K at pressures ranging from the vapor pressure of CO2 to approximately 15 MPa. These data were measured in a new analytical apparatus which is described in detail. The results are supported by a rigorous assessment of uncertainties and careful validation measurements. The new data help to resolve discrepancies between previous studies, especially for the (CO2 + H-2) system. Experimental measurements of the three-phase solid-liquid-vapor locus are also reported for both binary systems.

The vapor-liquid equilibrium data are modeled with the Peng-Robinson (PR) equation of state with two binary interaction parameters: one, a linear function of inverse temperature, applied to the unlike term in the PR attractive-energy parameter; and the other, taken to be constant, applied to the unlike term in the PR co-volume parameter. This model is able to fit the experimental data in a satisfactory way except in the critical region. We also report alternative binary parameter sets optimized for improved performance at either temperatures below 243 K or temperatures above 273 K. A simple predictive model for the three-phase locus is also presented and compared with the experimental data.

Graphical abstract

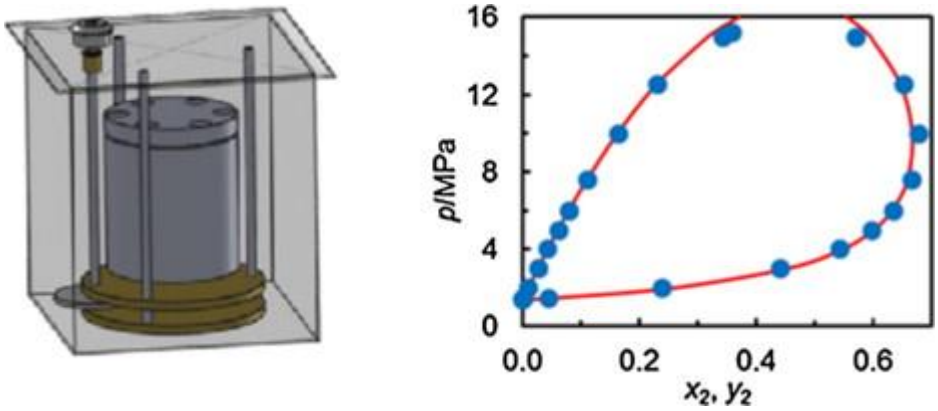

Highlights

► Measurements of vapor–liquid and solid–vapor–liquid equilibria. ► Mixtures of CO_2 with H_2 or N_2. ► Temperatures from 218 K to 303 K with pressures up to 15 MPa. ► Modeling with the Peng–Robinson equation of state. ► Applicable to low-temperature CO_2 capture from syngas and pipeline transportation.

Keywords : Carbon capture, Carbon dioxide, Hydrogen, Nitrogen, Solid-vapor-liquid equilibrium, Vapor-liquid equilibrium

1. Introduction

Gas separation processes are a mature area of chemical technology in which low-temperature flash and/or distillation processes play an important role. The design of such processes depends to a great extent upon the availability of reliable vapor-liquid and solid-vapor-liquid equilibrium data and this has stimulated a large number of experimental studies in this area. New requirements in the energy industry for the separation of CO_2 from either synthesis/fuel gases (pre-combustion) or flue gases (post combustion), associated with carbon capture and storage, have renewed and extended the requirements for relevant phase-equilibrium data. In the area of CO_2 separation from synthesis gas, a novel process involving cascaded low-temperature flash units has recently been patented [1]. This process is intended to separate the H_2 and CO_2 present in a shifted synthesis gas derived from gasification of coal or other feedstocks. A similar process, utilizing a distillation column instead of flash units, has been discussed in detail by Berstad et al. [2]. Processes of this kind will operate effectively in a region of low temperature and high pressure such that the feed stream separates into a CO_2-rich liquid phase and a H_2-rich gas phase. The available phase equilibrium data suggest that pressure of between (5 and 10) MPa and temperatures in the region of 220 K appears to be most suitable [2]. The key binary system in this case is (CO_2 + H_2), for which there is relatively little vapor-liquid equilibrium (VLE) data in the literature and some significant discrepancies between the sources that are available. The solid-vapor-liquid equilibrium (SVLE) locus of this system is also important as it sets the lowest possible operating temperature consistent with the avoidance of solids formation. In view of the importance of reliable VLE and SVLE data for (CO_2 + H_2), the present work was commissioned with the objective of performing new high-accuracy measurements and providing simple correlative models suitable for application in process design.

Real shifted synthesis gases will contain a number of other gases in addition to CO_2 and H_2. Of these, N_2 may be important, especially if gasification is carried out in air rather than oxygen. Accordingly, the binary system (CO_2 + N_2) was also studied in this work. The mixtures of CO_2 with gases including H_2 and N_2 are also of interest in CO_2 pipeline engineering where it is necessary to know the pressure-temperature phase envelope of the fluid mixture to design a pipeline for operation in e.g. the gas phase or the dense liquid/supercritical fluid region.

The available VLE data for the two binary systems of interest in this work are summarized in Table 1. The VLE region in the (CO_2 + H_2) system is bounded at low pressures by the vapor-pressure curve of CO_2, at high temperatures and pressures by the critical locus of the binary system and at low temperatures and high-pressures by the solid-vapor-liquid three-phase line. Different parts of this region have been studied by several authors [3-7]. Kaminishi and Toriumi [3] appear to have been the first workers to study this system and their measurements were made along five isotherms at temperatures between (233.15 and 298.15) K with pressures up to 20 MPa. Spano et al. [4] made VLE measurements, by a quasi-static analytic method, at temperatures between (219.9 and 289.9) K with pressures up to 20 MPa. Yorizane [5] reported VLE data at the single temperature of 273.15 K with pressures up to 37 MPa. The most comprehensive study is that of Tsang and Streett [6] who made measurements over almost the full region of VLE, extending in pressure to a maximum of 172 MPa and in temperature from 220 K to 290 K. They used a static-analytic method with phase sampling and composition measurements by gas chromatography (GC). They also studied the three phase SVLE curve

at pressures between (36 and 161) MPa and estimated the point at which it meets the VLE critical locus: T = 235 K and p = 198 MPa. Finally, Bezanehtak et al. [7] measured VLE along three isotherms at temperatures from (278.15 to 298.15) K with pressures up to 19 MPa using a quasi-static analytic apparatus with liquid-phase re-circulation and on-line analysis by GC. As discussed below when we compare our results with the literature, there are quite significant differences between the reported data for the (CO_2 + H_2) system. In the liquid phase, the compositions reported by Tsang and Streett deviate from most of the other reported data while, in the gas phase, there is substantial scatter. Accordingly, the primary objective of the present study was to resolve these discrepancies by means of new high-quality measurements extending in temperature from just above the triple-point temperature of CO_2 to just below the critical temperature of CO_2.

The VLE of (CO_2 + N_2) system has been investigated extensively [3, 5, 8-25], with most studies utilizing a static or quasi-static analytic method. The available data are summarized in Table 1. It is notable that there is no single study that spans the temperature range from the triple point to the critical point of CO_2. The SVLE curve of (CO_2 + N_2) has not been reported previously.

In the rest of this paper, we describe a new apparatus built for this study and present VLE and SVLE data measured for (CO_2 + H_2) and (CO_2 + N_2). Uncertainties are carefully quantified and the results of validation measurements are presented to support these. We adopt a simple modelling approach for the VLE based on a cubic equation of state that can easily be applied in process simulations.

2. Experimental

2.1 Apparatus

A new low-temperature vapor-liquid equilibrium (VLE) apparatus was constructed to measure the phase behavior of mixtures of CO_2 with components such as H_2, N_2 and other light gases. The apparatus had a maximum working pressure of 20 MPa and a working temperature range from 183 K to 473 K. The experimental technique was based on the static-analytical method in which samples of liquid and vapor coexisting in equilibrium at a given temperature and pressure were withdrawn and their compositions measured by gas chromatography. Fig. 1 is a schematic diagram of the apparatus of which the main parts are a gas-handling system, a VLE cell housed in a thermostat bath, and a gas chromatograph connected via sampling devices to the VLE cell.

The purpose of the gas handling system was to permit the following functions relating to the VLE cell: initial evacuation; filling with an approximately-known amount of CO_2; additional of up to four further gases; measurement of the pressures of the inlet gas supplies, and of the equilibrium pressure in the VLE cell; over-pressure protection of the VLE cell and CO_2 reservoir; and finally safe disposal of gases following use.

The VLE cell, fabricated from type 316L stainless steel, had an internal volume of 143 cm^3 and a maximum working pressure of 20 MPa at the maximum service temperature of 473 K. As shown in Fig. 2 (a), the vessel comprised a monobloc pot, a seal retaining ring and a flat-

plate closure retained by bolts that engaged threads machined in the wall of the pot. The seal was a nitrogen-pressurized gold-plated hollow stainless-steel O-ring (Busak & Shamban, Wills Ring, type O); this proved to be highly reliable.

The pressure was measured by means of a gauge pressure transmitter (Keller model PA-33X, 30 MPa full scale), providing both a digital (RS485) and analogue (0-10 Vdc) outputs, combined with an absolute ambient-pressure sensor (Keller model PAA-21Y, 0.2 MPa full scale). The analogue signal from the gauge pressure transmitter was used with a panel meter to provide a display but the digital output was used for data acquisition.

During an experiment, the VLE cell was immersed in a thermostatic fluid bath (Lauda Proline model RP890) which, for this work, was filled with ethanol. The contents of the VLE cell were stirred by a 25 mm long magnetic stirrer bar (follower), coupled to an external permanent magnet drive system rotated by a motor, drive shaft, and gear assembly as shown in Fig. 2 (b). The drive magnet assembly comprised two 10 mm diameter x 6 mm thick SmCo disc magnets, embedded in a nylon gear wheel and linked below by a mild-steel yoke. The motor was operated at speeds of up to 400 rpm. In order to reduce the risk of fire or explosion in the event of a leak, the enclosed space within the bath was purged with a continuous slow flow of nitrogen gas.

The thermostat bath was able to control the temperature with a stability of ±0.01 K over the time span of an isothermal experiment. The temperature of the VLE cell was measured by means of a calibrated Pt100 thermometer (Fluke model 5615) and digital readout (Fluke model 1502A).

The gas chromatograph (Agilent model 7890A) was equipped with a 10-port gas sampling valve fitted with dual sample loops for the injection of calibration gases, a packed column, and a thermal conductivity detector. The carrier gas was diverted prior to the 10-port valve via heated transfer lines to and from a pair of electromagnetic sampling valves (Rolsi model Evolution IV) used for withdrawing samples of the coexisting phases from the VLE cell. Initially, these valves were connected in series but this was later modified as shown in Fig. 1 so that the carrier gas flowed through both valves in parallel. For the system (CO_2 + H_2), argon was used as the carrier gas and the components were separated on a 3 m x 3.2 mm o.d. RT-Sulfur column. For the system (CO_2 + N_2), the same column was used but helium was the carrier gas.

Sampling of the vapor and liquid phases was accomplished by means of electromagnetic sampling valves (Rolsi Evolution IV) that were coupled to the VLE cell by 0.13 mm i.d. stainless-steel capillary tubes that passed through compression seals in the lid of the cell. The capillary for the liquid phase extended nearly to the bottom the cell, while that for the vapor projected about 10 mm below the inner face of the lid. The quantity of sample withdrawn was controlled by the programmable opening time which varied between 10 ms and 60 ms, depending upon the pressure.

The gas sampling loops (nominal volume 0.25 cm^3) were filled with calibration gases by means of automated solenoid valves. Pressure sensors (Keller model PAA-21Y, 0.6 MPa full scale)

were also fitted so that the pressure of the calibration gases could be determined prior to injection. The loops themselves were located in the thermostatted valve compartment within the GC where the temperature was also measured.

Referring to Fig. 1, valve V-1 was used to isolate the VLE cell from the rest of the gas-handling system. When open, V-1 allowed gases to flow from the gas handling-system to the VLE cell, or from the VLE cell to waste, or (at sufficiently low pressure) to the vacuum pump. Valve V-2 allowed CO_2 at the supply pressure of about 6 MPa to flow into the 0.5 dm^3 reservoir E2. This reservoir was protected by a burst-disc device venting to atmosphere. From the reservoir, CO_2 could be transferred to the VLE cell via valve V-3 and the quantity could be metered approximately by measuring the change in the pressure within the reservoir. A selector valve, V-4, allowed one of four additional gases to be selected for input through valve V-5. A pressure indicator connected between these two valves permitted measurement of the inlet gas pressure. To vent gases from the VLE cell, valve V-6 was opened and the gas then flowed to a propane burner. The purpose of the burner was to incinerate flammable and/or toxic components prior to releasing them into the laboratory fume extraction system. When the pressure remaining in the VLE cell was sufficiently low, V-6 could be closed and the remaining gas exhausted via V-7 through a two-stage diaphragm-type vacuum pump and thence to the waste-gas burner. A minimum pressure of 0.4 kPa could be achieved in this way.

2.2 Calibration and uncertainty analysis

The pressure transmitter used to measure the experimental pressure was calibrated by the manufacturer with a stated maximum uncertainty of 0.05 % of the full scale pressure (i.e. 0.015 MPa) over the working temperature range of (283 to 333) K. The calibration was checked at ambient temperature, approximately 296 K, by comparison with a primary pressure standard (Fluke model DHI PPCH-G) having a relative uncertainty of 0.016 % of reading. All measured data were found to be within ±0.009 MPa. Hysteresis was within ±0.001 MPa. A linear deviation function was determined that fitted all calibration data to within ±0.003 MPa. In use, the absolute pressure was obtained from the reading of the pressure transmitter by adding the ambient pressure measured within the same enclosure by means of the second sensor. The uncertainty associated with this sensor was less than 0.001 MPa. The overall standard uncertainty ascribed to the measured system pressure was 0.003 MPa.

The platinum resistance thermometer was calibrated on the International Temperature Scale of 1990 at temperatures between 77 K and 693 K by the manufacturer in January 2008 with standard uncertainty of 0.006 K in the temperature range of relevance here. Prior to the present work, which took place during 2012, the calibration of the sensor was checked in a triple-point-of-water cell and by comparison with a standard platinum resistance thermometer in a thermostatic bath at temperatures between 243 K and 448 K. The deviations found were within ±0.003 K. The calibration parameters were slightly amended to accommodate these shifts. The overall standard uncertainty ascribed to the temperature measurements was 0.006 K.

Calibration of the GC was accomplished primarily by an absolute area method in which samples of the pure gases were injected sequentially via the gas sampling valve and the area

response of the TCD was recorded. The filling pressure of the sample loops was varied between (0.1 and 0.4) MPa and the area response recorded for many repeated injections. With both carrier gases, slightly non-linear responses were observed and the calibration data were fitted with the following function

$$(n_i / V) = a_{i,1} A_i + a_{i,2} A_i^2 . \quad (1)$$

Here, n_i is the amount of pure substance i introduced in a given calibration injection, V is the volume of the sample loop, and $a_{i,1}$ and $a_{i,2}$ are calibration parameters. Since the volume of a given sample loop was constant, and mole fractions are calculated from ratios of amounts, the actual volume was immaterial. In the analysis, the molar density (n_i/V) was calculated from the equation of state of the substance in question. Fig. 3 shows the calibration data gathered for H_2 and CO_2 together with deviations of the data from Eq. (1).

The uncertainties associated with this calibration method have been discussed in detail by Al Ghafri et al. [26]. For the purposes of the uncertainty analysis, the small quadratic term in Eq. (1) is neglected and chromatographic response factors f_i are defined such that

$$n_i = f_i A_i . \quad (2)$$

It is shown in [26] that the uncertainty $u(x_i)$ in the mole fraction x_i associated with both the measurement and the calibration steps, but excluding the effects of uncertainties in temperature and pressure, is given by

$$u^2(x_i) = \left[x_i(1 - x_i)\right]^2 \sum_{j=1}^{2} \left[u_r^2(A_j) + u_r^2(f_j)\right]. \quad (3)$$

Here, $u_r(A_j)$ is the standard relative uncertainty in the peak area associated with component j and $u_r(f_j)$ is the standard relative uncertainty of the corresponding response factor as determined during calibration. The latter is given by

$$u_r^2(f_j) = \left[u_r^2(n_j) + u_r^2(A_j)\right]_{\text{cal}} , \quad (4)$$

where subscript 'cal' denotes calibration and $u_r(n_j)$ is the standard relative uncertainty of the amount of substance introduced in the calibration measurement. Since calibration gases were introduced from sample loops of fixed volume, and that volume cancels out exactly in the determination of a mole fraction, $u_r(n_j)$ may be equated with the standard relative uncertainty of the gas density in the sample loop, which is related in turn to the uncertainties of the filling temperature and pressure and, in principle, to the uncertainty in the equation of state of the gas. The latter is negligible and the uncertainty in the loop temperature and pressure (1 K and 0.001p, respectively) lead to $u_r(n_j)$ = 0.3 %. The standard relative uncertainty of the chromatographic areas was estimated from the relative standard deviation of repeated measurements at the same filling conditions. Often, this quantity was < 0.1 % but, to accommodate the scatter of the least repeatable measurements, we take this to be 0.5 %. This analysis implies that $u_r(f_j) \approx 0.6$ % for all components.

During measurements, Rolsi samplers were used and these do not provide samples of exactly repeatable size, Consequently, it was not possible to determine the repeatability of the absolute chromatographic peak area. However, from the repeatability of the mole fractions, we deduce that the standard relative uncertainty of the peak areas during sampling was similar

to that found during calibration, *i.e.* 0.5 %. Combining terms, the estimated standard uncertainty reduces to the following simple expression

$$u(x_i) = 0.011 \cdot x_i(1 - x_i) \,. \tag{5}$$

For very small mole fractions, a minimum uncertainty of 5 x 10^{-5} is estimated. We remark that the repeatability of the measurements at fixed sample size was often one order of magnitude better than the estimated overall uncertainty and that improved calibration methods might lead to a significant reduction in the composition uncertainty.

2.3 Materials and methods

The gases used in this work are detailed in Table 2; all were used as supplied. Additional reference gas mixtures were employed to validate the GC system; these were prepared gravimetrically by the supplier (SIP Analytical Ltd) and certified with a mole-fraction uncertainty of 0.01*x*, where *x* is the mole fraction of the minor component.

Prior to each isothermal run, the VLE cell was flushed with CO_2 and evacuated several times. Sufficient CO_2 to approximately half fill the vessel with liquid was then introduced and the system brought into thermal equilibrium under stirring. Equilibrium was assessed by monitoring both the temperature and the pressure. The vapor pressure of the CO_2 was then compared with the prediction of the reference equation of Span and Wagner [27]. If the measured vapor pressure deviated from the reference equation by more than the combined uncertainty then the sample was vented and vessel flushed again. Once an acceptable vapor pressure was recorded, H_2 or N_2 was admitted to increase the pressure, and the system again brought into equilibrium under stirring. Samples of the vapor and liquid phases were then withdrawn and analyzed by GC. Because of 'stagnant' gas in the sampling capillary, the first sample from a given phase was always ignored. Typically a further five samples were then taken over a period of 30 min and checked for repeatability. If there was any sign of drift then a further period of equilibration was allowed and the sampling process repeated. The amount withdrawn from the cell in each sampling operation was such that even 10 such operations had an insignificant effect of the pressure and hence on the position of equilibrium. After determining the composition of both phases, additional gas was admitted to raise the pressure further and the process repeated until either the maximum supply pressure or the critical pressure of the system was reached. This procedure was generally reliable and straight forward except near to the critical point where, if the initial charge of CO_2 was not correctly chosen, the overall composition could pass out of the two phase region before the critical point was reached. In these cases, a trial-and-error approach was followed to stay inside the phase envelope.

The points along the three phase (S + V + L) line were determined for various mixtures of fixed overall composition by studying the pressure-temperature relation during a controlled isochoric cooling ramp. In these experiments, the bath was programed to cool at a rate of 1 $K \cdot h^{-1}$ while the bath temperature and temperature and pressure data from the VLE cell were continually logged. Fig. 4 (a) shows both temperature readings and the pressure as functions of time *t* during such a cooling ramp in the (CO_2 + H_2) system. During the early part of the data segment shown, a small temperature difference is evident between the bath and the cell,

consistent with heat flowing out from the VLE cell and its contents. Nucleation of freezing is evident from a change in slope of in $p(t)$. The extent of supercooling is illustrated in Fig. 4 (b), where pressure is plotted against the cell temperature. The $p(T)$ curve initially follows a path in the stable two-phase (V + L) region; this path is extended into a metastable (V + L) region, before nucleation occurs, the temperatures rises and the $p(T)$ path continues in the stable three-phase (S + V + L) region. The equilibrium phase boundary between two- and three-phase regions was reconstructed by extrapolation of $p(T)$ curve, as shown, from the stable three-phase path. Fig. 4(c) and Fig. 4(d) show data from a similar isochoric cooling ramp measured in (CO_2 + N_2). In this case, freezing is accompanied by a rise in pressure indicating that the molar volume of the solid phase is greater than that of the coexisting liquid.

2.4 Validation

Several validation tests were carried out. First, the vapor pressure of pure CO_2 was measured at temperatures from just above the triple point to just below the critical point. The results are compared with the predictions of the reference equation of state of Span and Wagner [27] in Fig. 5. In no case did the deviation exceed the combined uncertainty of the experimental measurement and the equation of state. Second, reference gas mixtures were employed to validate the GC system and its calibration. For (CO_2 + H_2), a mixture containing 90 mol% H_2 was tested while, for (CO_2 + N_2), an equimolar mixture was studied. The test gases were introduced both via the sample loops and gas sampling valve within the GC and from the gas-filled equilibrium vessel by means of the Rolsi samplers. The results, representing the mean of repeated injections, are given in Table 3 in comparison with the certified mixture composition. The difference between the measured and certified mole fraction was well within the combined standard uncertainty.

3. Modelling approach

In order to provide a convenient correlation of the phase behavior of the systems studied, the results were regressed to determine binary interaction parameters for use in the standard Peng-Robinson equation of state:

$$p = \frac{RT}{V_m - b} - \frac{a(T)}{V_m(V_m + b) + b(V_m - b)}. \tag{6}$$

Here, p, V_m and T are pressure, molar volume, and temperature, R is the universal gas constant, and a and b are the energy and co-volume parameters which, for a pure substance, are given as follows:

$$a(T) = 0.457235\,(RT_c)^2 \alpha(T) / p_c, \tag{7}$$

$$\alpha(T) = \left[1 + \left(0.37464 + 1.54226\,\omega - 0.26992\,\omega^2\right)\left(1 - \sqrt{T/T_c}\right)\right]^2, \tag{8}$$

$$b = 0.077796\,RT_c / p_c, \tag{9}$$

where p_c, T_c and ω are the critical pressure, critical temperature and acentric factor, respectively. To apply the model to mixtures, we employ the classical one-fluid mixing rules:

$$a = \sum_i \sum_j x_i x_j (1 - k_{ij}) \sqrt{a_i a_j} \tag{10}$$

$$b = \sum_i \sum_j x_i x_j (1 - l_{ij})(b_i + b_j)/2\,, \tag{11}$$

where k_{ij} and l_{ij} are binary interaction parameters (non-zero only when $i \neq j$) [28]. In this work, we correlate k_{ij} as a linear function of inverse temperature,

$$k_{ij} = k_{ij,0} + k_{ij,1}/T\,, \tag{12}$$

while l_{ij} is either zero or constant, leading to up to three adjustable parameters per binary mixture. A temperature-dependent correlation for l_{ij} was not considered because this can lead to unphysical behavior such as $p(V_m)$ isotherms crossing.

When regressing the binary parameters against experimental data, it is common to take T and the liquid-phase mole fraction x_2 as the independent (given) variables and to calculate p and the vapor-phase mole fraction y_2 at each state point. The objective function is then based on a combination of the squared deviations of the experimental p and y_2 from these calculated values. In this work, we note that the temperature and pressure, being associated with very small uncertainties, are more suitable as the given quantities. Accordingly, the objective function used was

$$S^2 = \frac{1}{N}\sum_{i=1}^{N}\left[(x_{2,i} - x_{2,i,\mathrm{calc}})^2 + (y_{2,i} - y_{2,i,\mathrm{calc}})^2\right], \tag{13}$$

where subscript i identifies a state point, subscript 'calc' denotes a value calculated from the thermodynamic model, and N is the total number of state points. Alternative objective functions could be devised, especially one in which the mole-fraction deviations are normalized by the experimental uncertainty. However, we prefer to proceed with Eq. (13) which accords to all state points equal weight.

Coexisting-phase compositions were determined from the equality of partial fugacity criterion. For the chosen equation of state and mixing rules, the partial fugacity coefficient φ_i of component i in a given phase is given by [28]

$$\begin{aligned}\ln\varphi_i = {} & (z-1)\left[2\sum_j\left(\frac{x_j b_{ij}}{b}\right) - 1\right] - \ln(Z - B) \\ & - \frac{A}{2\sqrt{2}B}\left[2\sum_j\left(\frac{x_j a_{ij}}{a}\right) - 2\sum_j\left(\frac{x_j b_{ij}}{b}\right) + 1\right]\ln\left[\frac{Z + (1+\sqrt{2})B}{Z + (1-\sqrt{2})B}\right],\end{aligned} \tag{14}$$

where $Z = pV_m/RT$, $A = ap/(RT)^2$ and $B = bp/RT$.[1]

Two factors significantly complicate the representation of the VLE data by means of a cubic equation of state, such as the Peng Robinson equation. The first arises for H_2 which behaves as a quantum fluid at low temperatures (e.g. near and below its critical temperature) but as a classical fluid in the temperature range of interest here. This results in poor performance of the model when the parameters of the equation of state are obtained from the critical constants and acentric factor as dictated by Eqs (7) to (9). This problem can be circumvented by using effective values of T_c, p_c and ω as proposed by Gunn et al. [29] and/or by using a modified

[1] Equation (34) of reference [28] has incorrect coefficients of B in the final logarithmic factor; this has been corrected in our equation (14).

function for $\alpha(T)$. In this work, the standard $\alpha(T)$ function was used and effective values of T_c, p_c and ω were obtained by fitting the model to the second B_2 [30] and third B_3 [31-35] virial coefficients of normal H_2 at temperatures between (65 and 500) K. For the Peng-Robinson equation, the pertinent relations are:

$$\left.\begin{aligned} B_2 &= b - a/(RT) \\ B_3 &= b^2 + 2ab/(RT) \end{aligned}\right\}. \tag{15}$$

As shown in Fig. 6, adjustment of T_c, p_c and ω resulted in a good representation of the second virial coefficient and an adequate representation of the third virial coefficient in the temperature range of the present work. Table 4 lists the critical (or effective) critical constants and acentric factors used for the three components studied [27, 36].

The second problem, common to all analytical thermodynamic models, is that the equation of state cannot represent experimental data close to a critical point. This problem may be addressed by means of a cross-over model [37] but we have not applied such an approach as it involves considerable complexity and only a few of the isotherms extent to the critical pressures. Accordingly, the Peng-Robinson model as applied cannot be expected to represent the near critical behavior. In order to avoid biasing the fitted PR models, we excluded some experimental points in the near critical region from the calculation of the objective function with Eq. (13).

The experimental data at temperatures approaching the critical temperature of CO_2 can nevertheless be fitted by an empirical function that includes a non-analytical term of approximately the theoretically-predicted form as follows:

$$\left.\begin{aligned} \tfrac{1}{2}(y_2 - x_2) &= c_1(z-1) + c_2(z^2-1) + c_3(z^\beta - 1) \\ \tfrac{1}{2}(y_2 + x_2) &= c_4(z-1) + c_5(z^2-1) + c_6(z^\beta - 1) \end{aligned}\right\}. \tag{16}$$

Here, $z = (p_c - p)/(p_c - p_{sat})$, p_{sat} is the vapor pressure of pure CO_2 at the temperature in question, $\beta = 0.325$, c_1 satisfies the constraint $c_1 = (c_2 + c_3)$, and the critical composition is given as $x_{1,c} = 1 - (c_4 + c_5 + c_6)$. The value of such fitting is that estimates of the critical pressure and composition may be obtained from the experimental data.

In order to model the three-phase (S + V + L) coexistence curve, we adopt a simple model in which the solid phase is treated as pure crystalline CO_2 and the coexisting liquid is treated as an ideal mixture of real fluids. The latter assumption, implies that the fugacity f_1^L of CO_2 in the liquid phase is given by

$$f_1^L = x_1 p \exp(G_{1,res}^L / RT), \tag{17}$$

where $G_{1,res}^L$ is the molar residual Gibbs free energy of pure liquid carbon dioxide. The fugacity of the solid phase is $f_1^S = p\exp(G_{1,res}^S / RT)$, where $G_{1,res}^S$ is the molar residual Gibbs free energy of pure solid carbon dioxide. In this work, we evaluate $G_{1,res}^L$ and $G_{1,res}^S$ from the equations of state of Span and Wagner [27] (for the fluid phases) and Trusler [38] (for the solid phase), and we make use of the Peng-Robinson model for the purposes of evaluating $x_1(T, p)$. Three-phase states were then predicted at given pressure by adjusting the temperature so as to equate the fugacity of pure solid CO_2 with the partial fugacity of CO_2 in the liquid mixture having

the mole fraction $x_1(T, p)$ predicted at (V + L) coexistence. The advantage of this hybrid model, involving as it does two fluid-phase equations of state, is that the predicted three-phase curves pass exactly through the triple-point of pure CO_2. In contrast, the (V + L) coexistence temperature of pure CO_2 predicted by the PR EoS is too high by about 0.8 K at the experimental triple-point pressure and, if this model alone is used for fluid phases, then the same error propagates into predictions of the three-phase line of the binary mixtures.

4. Results and discussion

4.1 (CO_2 + H_2) system

The (V + L) phase behavior of the (CO_2 + H_2) system was measured along 9 isotherms at temperatures from just above the triple-point temperature to just below the critical temperature of CO_2, at pressures from the vapor pressure of CO_2 to approximately 15 MPa. The results are given in Table 5. As noted above a few near-critical state points are not included in the subsequent analysis and these are identified in Table 5.

To correlate the VLE data, we employed the PR EoS first with the binary parameter l_{12} in Eq. (11) taken as zero. This conventional approach provides a reasonable correlation of the data, except in the region of the critical pressure (which was only approached on two isotherms). The binary parameters and the value of the objective function obtained in this fit are given in Table 6. Unfortunately, this model systematically overestimates the mole fractions in both liquid and vapor phases and even a more-complex temperature dependence for k_{12} does not improve the situation. A significantly better correlation is obtained by including l_{12} in the fit and the optimized parameters obtained in this case are also given in Table 6; in this case, the objective function (S^2) is smaller by a factor of 3.8. Slightly improved fits could be obtained by adjusting k_{12} and l_{12} on individual isotherms or by applying Eqs (10) and (11) in sub-intervals of temperature. For example, the results obtained with the analysis restricted to the three lower-temperature isotherms are also given in Table 6. It is notable that k_{12} for this system is far from zero, varying from -0.52 at the lowest temperature to -0.84 at the highest temperature, indicating that the unlike attractive interactions are much stronger than implied by the Berthelot rule.

In Figs 7(a) to 7(h), we plot the experimental data measured on the lower eight of the nine isotherms studied. The PR correlation, based on use of Eqs (10) and (11) with the recommended values of $k_{12,0}$, $k_{12,1}$ and l_{12} from Table 6, is also plotted in these figures. One can observe generally very good agreement, except in Fig. 7(h) close to the critical pressure. The isotherm at T = 303.15 K is only 1 K below the critical temperature of pure CO_2 and the (V + L) coexistence region, plotted separately in Fig. 8, is rather small. We note that the PR model overestimates the critical composition and pressure and generally fails, as expected, to follow the experimental data near to the critical point. On the other hand, as shown in both Fig. 7(h) and Fig. 8, the near-critical data can be represented very well by Eq. (16). The values of the critical pressure and composition so determined, along with the other parameters in Eq. (16), are given in Table 7.

In Fig. 9, we compare the present experimental VLE results and data from the literature as deviations from the PR model with the recommended values of $k_{12,0}$, $k_{12,1}$ and l_{12} from Table 6. The plots show separately the deviations of experimental liquid and vapor compositions from the predictions of the model at given T and p, and are separated into two regions corresponding to temperature below and above 275 K. If we consider first the present experimental results in detail, we see smooth systematic deviations from the model that are generally much larger than the experimental uncertainties. In the liquid phase, the mole fractions of H_2 is generally under predicted at low temperatures and at high pressures. Conversely, the H_2 mole fractions are generally over predicted in the vapor phase at low temperatures and pressures. This is most probably attributable to the failure of the standard PR equation to reproduce accurately the vapor pressure of pure CO_2. The magnitude of the deviations are generally larger in the vapor phase than in the liquid and, for both phases, large deviations can be seen in the approach to the critical point at the highest temperature.

In comparison with the literature [3-7], there is generally good agreement at low temperatures in the liquid phase (see Figs 9a and 9c) with the exception of the results of Tsang and Streett [6] which deviate systematically from the other data in both phases. At temperatures above 275 K the data of Bezanehtak et al. [7] follow those Tsang and Street [6], while the data of Spano et al. [4] and Kaminishi and Toriumi [3] agree with our results. As noted above, the vapor phase data are generally more scattered and this is especially evident at higher temperatures. However, as shown in Fig. 9(d), the vapor-phase data of Tsang and Street are in better agreement with the present results in this region. It is not obvious why the data from reference [6] deviate from the present results in the liquid phase but agree much better in the vapor phase, especially at higher temperatures.

The three-phase (S + V + L) boundary was studied by means of three cooling ramps starting with pressures of approximately (5, 10 and 15) MPa. The three-phase states determined in this way are reported in Table 8 and plotted, along with the triple-point and melting curve of pure CO_2 in Fig. 10. The estimated standard uncertainty of the melting temperature, at given pressure, is 0.1 K reflecting mainly the need to extrapolate the cooling curve from below the phase transition temperature to account for the effects of super-cooling. The experimental data are found to be in excellent agreement with the predictions of the model discussed above. Note that this model contains no adjustable parameters; however, in the PR model, we use the binary coefficients from Table 6 pertaining to the lower three VLE isotherms alone to predict more accurately the composition of the liquid phase.

4.2 (CO_2 + N_2) system

The (V + L) phase behavior of the (CO_2 + N_2) system was measured along 7 isotherms spanning the same temperature interval as studied for (CO_2 + H_2). The results are given in Table 9 and plotted in Fig. 11. The few near-critical state points not included in the subsequent analysis are identified by footnote in Table 9. The data were correlated with the PR EoS model in exactly the same way as described above and the binary coefficients are given in Table 6. In this system, the improvement associated with inclusion of the l_{12} binary parameter in Eq. (11) is less pronounced but still significant. Compared with (CO_2 + H_2), the (CO_2 + N_2) system exhibits a lower critical pressure locus and consequently a greater part of the experimental

data falls in the critical region leading to slightly poorer fitting. Note however, that the objective function S excludes experimental data close to the critical points on the isotherms that reach or approach the critical locus. Overall, the PR model correlates the data in a satisfactory way except at the highest temperature.

As shown in Fig. 8, the region of VLE at T = 303.15 K is even smaller than found for the (CO_2 + H_2) system. Again, the data are well fitted by the empirical model (Eq. 16) and the parameters determined from the isotherms at (288.65 and 303.15) K, including the critical pressure and composition, are given in Table 7.

The present experimental results are compared with data from the literature and with the PR model in Fig. 12. Our results again exhibit small, relatively smooth, systematic deviations which we attribute to the two short-comings of the PR model: failure to reproduce the vapor pressure of pure CO_2; and inaccurate behavior in the critical region. For this system there is a large body of data in the literature, much of it in fair agreement with the present study. The data of Bian et al. [22] at temperatures of 301.3 K and 303.3 K deviate significantly from both the present results and the Peng-Robinson model, although those reported earlier by Bian [19] are in quite good agreement.

5. Pressure-temperature phase envelopes

For problems involving streams of fixed composition, it is often convenient to consider the pressure-temperature phase envelopes. In particular, for CO_2 pipeline engineering problems involving impure CO_2, the p-T phase envelope of the mixture is needed in the temperature range of interest, typically ≥ 270 K. For a single impurity of either H_2 or N_2, the phase envelopes may be obtained from the present experimental data by means of interpolation on each isotherm over the relevant ranges of composition. Table 10 lists the dew and bubble pressures obtained in this way for both systems at CO_2 mole fractions of 0.95 and 0.98; these were obtained by quadratic interpolation of the VLE data on each isotherm at x_1 ≥ 0.93. The interpolated experimental data are plotted in Fig. 13, along with the vapor-pressure curve of pure CO_2 and the experimental critical locus (the latter from Table 7). Both H_2 and N_2 move the two-phase region to pressures above the vapor pressure curve of pure CO_2. Predicted value of the bubble and dew curves calculated from the Peng-Robinson model with the recommended binary interaction parameters from Table 6 are in fair agreement with these values; however, the bubble pressures are slightly over predicted. The over prediction of the bubble pressure is most notable for (CO_2 + H_2) and can be discerned in Fig. 7. Improved agreement with the interpolated experimental data was obtained by refitting the binary parameters to the experimental data in the regions T ≥ 273 K and x_1 ≥ 0.93. In this case, it was not necessary to include a temperature dependence for k_{12} and, in the case of the (CO_2 + N_2) system, a non-zero value of l_{12} was not required. These binary parameters are given in Table 6 and Fig. 13 shows that, with these values, the Peng-Robinson model provides a good representation of the interpolated experimental dew- and bubble-point data, except close to the critical locus for (CO_2 + H_2) where the critical point is over predicted.

6. Conclusions

The present study addresses the phase behavior of the binary mixtures (CO_2 + H_2) and (CO_2 + N_2) over the full range of coexistence temperatures at pressures up to approximately 15 MPa, thereby covering the regions of interest in both low-temperature syngas separations and CO_2 pipeline engineering. The measurements were carried out in a new apparatus and are believed to have significantly lower uncertainties than previous studies. A simple model, based on the Peng-Robinson equation of state with two binary interaction parameters, is shown to give a fair account of the data. The model fails marginally in the vapor phase at low pressures, presumably because it does not quite match the vapor pressure of pure CO_2, and in the critical region. The former deficiency might be corrected with an improved $\alpha(T)$ function in place of Eq. (8), while correction of the latter requires a crossover model. We provide for each system several alternative sets of parameters in the Peng-Robinson model: one representing the best fit over the whole experimental range (excluding a few near-critical points); and others specialized to either low temperatures or temperatures above 270 K with $x_1 \geq 0.93$.

We also report data on the SVLE locus in both (CO_2 + H_2) and (CO_2 + N_2), the latter being studied for the first time. We test a simple model based on the assumptions that the solid phase is pure CO_2 and that the liquid may be treated as an ideal mixture of non-ideal fluids. This gives excellent predictions for (CO_2 + H_2) but deviates somewhat from the experimental data for (CO_2 + N_2).

Acknowledgements

This work was carried out as part of the CCS Next Generation Capture Technology project, commissioned and funded by the Energy Technologies Institute. We are pleased to acknowledge support for this work provided by Costain Natural Resources. We also acknowledge the contribution of Dr Niall McGlashan to the modelling of experimental data.

References

[1] S.R. Jackson, C. Corden, P.W. Howells, inventors; Costain Oil, Gas & Process Ltd, assignee. Process and Apparatus for the Separation of Carbon Dioxide and Hydrogen. Patent GB 2490476-A (2012)

[2] D. Berstad, P. Nekså, G.A. Gjøvåg, Low-temperature syngas separation and CO_2 capture for enhanced efficiency of IGCC power plants, Energy Procedia, 4 (2011) 1260-1267.

[3] G.I. Kaminishi, T. Toriumi, Vapor-liquid phase equilibrium in the CO_2 - H_2, CO_2 - N_2 and CO_2 - O_2 System, Kogyo Kagaku Zasshi, 69 (1966) 175-178.

[4] J.O. Spano, C.K. Heck, P.L. Barrick, Liquid-vapor equilibria of the hydrogen - carbon dioxide system, J. Chem. Eng. Data, 13 (1968) 168-171.

[5] M. Yorizane, The determination of vapor-liquid equilibrium data at high pressure and low temperatures, Asahi Garasu Kogyo Gijutsu Shoreikai Kenkyu Hokoku, 18 (1971) 61-76.

[6] C.Y. Tsang, W.B. Streett, Phase equilibria in the H_2 - CO_2 system at temperatures from 220 to 290 K and pressures to 172 MPa, Chem. Eng. Sci., 36 (1981) 993-1000.

[7] K. Bezanehtak, G.B. Combes, F. Dehghani, N.R. Foster, D.L. Tomasko, Vapor-liquid equilibrium for binary systems of carbon dioxide + methanol, hydrogen + methanol, and hydrogen + carbon dioxide at high pressures, J. Chem. Eng. Data, 47 (2002) 161-168.

[8] I.R. Krichevskii, N.E. Khazanova, L.S. Lesnevskaya, L.Y. Sandalova, Vapor-liquid equilibrium at high pressure in the system nitrogen - carbon dioxide, Khim. Promst. Moscow, (1962) 169-171.

[9] G.H. Zenner, L.I. Dana, Liquid-vapor equilibrium compositions of carbon dioxide - oxygen - nitrogen mixtures, Chem. Eng. Progr. Symp. Ser., 59 (1963) 36-41.
[10] M. Yorizane, S. Yoshimura, H. Masuoka, Vapor-liquid equilibrium at high pressure: N_2 - CO_2, H_2 - CO_2 system, Kagaku Kogaku, 34 (1970) 953-957.
[11] T.A. Al-Sahhaf, A.J. Kidnay, E.D. Sloan, Liquid + vapor equilibria in the N_2 + CO_2 + CH_4 system, Ind. Eng. Chem. Fundamentals, 22 (1983) 372-380.
[12] W. Weber, S. Zeck, H. Knapp, Gas solubilities in liquid solvents at high pressures: apparatus and results for binary and ternary systems of N_2, CO_2 and CH_3OH, Fluid Phase Equilib., 18 (1984) 253-278.
[13] M. Yorizane, S. Yoshimura, H. Masuoka, Y. Miyano, Y. Kakimoto, New procedure for vapor-liquid equilibria. Nitrogen + carbon dioxide, methane + Freon 22, and methane + Freon 12, J. Chem. Eng. Data, 30 (1985) 174-176.
[14] G. Trappehl, Experimental study of vapor-liquid phase equilibria and caloric properties at low temperatures and high pressures with mixtures consisting of N_2, CH_4, C_2H_6, C_3H_8 and CO_2, Dissertation, TU Berlin, (1987) 1-237.
[15] T.S. Brown, V.G. Niesen, E.D. Sloan, A.J. Kidnay, Vapor-liquid equilibria for the binary systems of nitrogen, carbon dioxide, and n-butane at temperatures from 220 to 344 K, Fluid Phase Equilib., 53 (1989) 41821.
[16] T.S. Brown, E.D. Sloan, A.J. Kidnay, Vapor-liquid equilibria in the nitrogen + carbon dioxide + ethane system, Fluid Phase Equilib., 51 (1989) 299-313.
[17] T.A. Al-Sahhaf, Vapor-liquid equilibria for the ternary system N_2 + CO_2 + CH_4 at 230 and 250 K, Fluid Phase Equilib., 55 (1990) 159-172.
[18] X. Yang, Contribution to the experimental investigation and calculation of vapor-liquid phase equilibria, Dissertation, TU Berlin, (1991) 1-189.
[19] B. Bian, Measurement of phase equilibria in the critical region and study of equation of state, Thesis, University of Nanjing, (1992) 24838.
[20] N. Xu, J. Dong, Y. Wang, J. Shi, High pressure vapor liquid equilibria at 293 K for systems containing nitrogen, methane and carbon dioxide, Fluid Phase Equilib., 81 (1992) 175-186.
[21] N. Xu, J. Dong, Y. Wang, J. Shi, Vapor liquid equilibria for N_2 - CH_4 - CO_2 system near critical region, Huagong Xuebao, 43 (1992) 640-644.
[22] B. Bian, Y. Wang, J. Shi, Simultaneous determination of vapor-liquid equilibrium and molar volumes for coexisting phases up to the critical temperature with a static method, Fluid Phase Equilib., 90 (1993) 177-187.
[23] T.S. Brown, E.D. Sloan, A.J. Kidnay, Vapor-liquid equilibria for the ternary system N_2 + CO_2 + n-C_4H_{10} at 250 and 270 K, Int. J. Thermophys., 15 (1994) 1211-1219.
[24] B. Yucelen, A.J. Kidnay, Vapor-liquid equilibria in the nitrogen + carbon dioxide + propane system from 240 to 330 K at pressures to 15 MPa, J. Chem. Eng. Data, 44 (1999) 926-931.
[25] Z. Zhang, L. Guo, X. Yang, H. Knapp, Vapor and liquid equilibrium for nitrogen - ethane - carbon dioxide ternary system, Huagong Xuebao, 50 (1999) 392-398.
[26] S.Z. Al-Ghafri, E. Forte, G.C. Maitland, J.J. Rodriguez-Henríquez, J.P.M. Trusler, Experimental and Modeling Study of the Phase Behavior of (Methane + CO_2 + Water) Mixtures, J. Phys. Chem. B, Accepted (2015).
[27] R. Span, W. Wagner, A New Equation of State for Carbon Dioxide Covering the Fluid Region from the Triple-Point Temperature to 1100 K at Pressures up to 800 MPa, J. Phys. Chem. Ref. Data, 25 (1996) 1509-1596.
[28] T.Y. Kwak, G.A. Mansoori, Vanderwaals Mixing Rules for Cubic Equations of State - Applications for Supercritical Fluid Extraction Modeling, Chem Eng Sci, 41 (1986) 1303-1309.
[29] R.D. Gunn, P.L. Chueh, J.M. Prausnitz, Prediction of thermodynamic properties of dense gas mixtures containing one or more of the quantum gases, AIChE J., 12 (1966) 937-941.
[30] J.H. Dymond, K.N. Marsh, R.C. Wilhoit, K.C. Wong, Virial Coefficients of Pure Gases, in: M. Frenkel, K.N. Marsh (Eds.) Virial Coefficients of Pure Gases and Mixtures, Springerr-Verlag, Heidelberg, 2002.
[31] H.K. Onnes, C. Braak, Isotherms of Diatomic Gases and Their Binary Mixtures VII. Isotherms of Hydrogen between 0 deg C and 100 deg C, Communs. Phys. Lab. Univ. Leiden, 100b (1907).
[32] L. Holborn, J. Otto, Isotherms of several gases between +400 and -183 C, Z. Phys., 33 (1925) 1-11.

[33] T.T.H. Verschoyle, Isotherms of hydrogen, of nitrogen, and of hydrogen-nitrogen mixtures, at 0 degrees and 20 degrees C, up to a pressure of 200 atmospheres., Proc. R. Soc. London, A111 (1926) 552-576.
[34] A. Michels, W. de Graaff, T. Wassenaar, J.M.H. Levelt Sengers, P. Louwerse, Compressibility Isotherms of Hydrogen and Deuterium at Temperatures between -175 °C and +150 °C (at Densities up to 960 Amagat), Physica, 25 (1959) 25-42.
[35] S. Mihara, H. Sagara, Y. Arai, S. Saito, The Compressibility Factors of Hydrogen-Methane, Hydrogen-Ethane and Hydrogen-Propane Gaseous Mixtures, J. Chem. Eng. Jpn., 10 (1977) 395-399.
[36] R. Span, E.W. Lemmon, R.T. Jacobsen, W. Wagner, A. Yokozeki, A reference equation of state for the thermodynamic properties of nitrogen for temperatures from 63.151 to 1000 K and pressures to 2200 MPa, J. Phys. Chem. Ref. Data, 29 (2000) 1361-1433.
[37] M.A. Anisimov, J.V. Sengers, Critical Region, in: J.V. Sengers, R.F. Kayser, C.J. Peters, H.J. White (Eds.) Equations of State for Fluids and Fluid Mixtures 2000, pp. 381-434.
[38] J.P.M. Trusler, Equation of State for Solid Phase I of Carbon Dioxide Valid for Temperatures up to 800 K and Pressures up to 12 GPa, J. Phys. Chem. Ref. Data, 40 (2011) 043105.
[39] F.A. Somait, A.J. Kidnay, Liquid-vapor equilibria at 270.00 K for systems containing nitrogen, methane, and carbon dioxide, J. Chem. Eng. Data, 23 (1978) 301-305.

Table 1. Summary of the literature data available for the vapor-liquid equilibria of the systems (CO_2 + H_2) and (CO_2 + N_2).

Authors	T_{min}/K	T_{max}/K	p_{max}/MPa	Reference
		CO_2 + H_2		
Kaminishi and Toriumi	233.15	298.15	20	[3]
Spano et al.	219.9	289.9	20	[4]
Yorizane	273.15	273.15	37	[5]
Tsang and Streett	220	290	172	[6]
Bezanehtak et al.	278.15	298.15	19	[7]
		CO_2 + N_2		
Krichevskii et al	288.15	303.15	10	[8]
Zenner and Dana	218.15	273.15	13	[9]
Kaminishi and Toriumi	253.15	293.15	13	[3]
Yorizane et al.	273.15	298.15	12	[5, 10, 13]
Al-Sahhaf et al.	220	240	17	[11, 17]
Weber et al.	223.15	273.15	10	[12]
Trappehl	220	220	14	[14]
Brown et al.	220	270	14	[15, 16, 23]
Yang	220	253.15	14	[18]
Bian	293.1	298.8	9	[19]
Bian et al.	301.3	303.3	8	[22]
Xu et al.	288.3	298.4	10	[20, 21]
Yucelen and Kidnay	240	270	12	[24]
Zhanzhu et al.	220	253.15	5	[25]

Table 2. Description of chemical samples.

Chemical name	Source	Specified mole fraction Purity
Carbon dioxide	BOC	0.999 5
Hydrogen	BOC	0.999 99
Nitrogen	BOC	0.999 992
Argon	BOC	0.999 99
Helium	BOC	0.999 99

Table 3. GC validation measurements where x_2 denotes mole fraction of component 2 and Δx is the difference between the certified and the measured mole fraction. [a]

Gas	x_2 (certified)	x_2 (measured)	Δx	Injection method
CO_2 (1) + H_2 (2)	0.8998 ± 0.0010	0.8993	0.0005	Sample loop
CO_2 (1) + H_2 (2)	0.8975 ± 0.0010	0.8970	-0.0005	Rolsi
CO_2 (1) + N_2 (2)	0.5008 ± 0.0050	0.4998	-0.0010	Sample loop
CO_2 (1) + N_2 (2)	0.5008 ± 0.0050	0.4990	-0.0018	Rolsi

[a] Standard uncertainties are $u(x) = 0.001$ for $x \approx 0.9$ and $u(x) = 0.003$ for $x \approx 0.5$

Table 4. Critical (or effective critical) temperature T_c and pressure p_c, and acentric factor ω of the experimental fluids.

Components	T_c/K	p_c/MPa	ω	Ref.
CO_2	304.13	7.3773	0.22394	[27]
H_2	31.76	1.276	-0.0626	This work
N_2	126.19	3.3958	0.0372	[36]

Table 5. Experimental VLE data for the system CO_2 (1) + H_2 (2) at temperatures T and pressures p, where x denotes mole fraction in the liquid phase, y denotes mole fraction in the gas phase, and u denotes standard uncertainty. [a]

T/K	p/MPa	x_2	y_2	T/K	p/MPa	x_2	y_2
218.159 [b]	0.5584	0.0000	0.0000	273.190	4.6730	0.0082	0.1679
218.174	0.9625	0.0009	0.3928	273.190	5.3010	0.0124	0.2299
218.166	1.4769	0.0024	0.5927	273.192	6.2540	0.0189	0.3043
218.150	1.9503	0.0036	0.6791	273.194	7.6130	0.0281	0.3810
218.181	3.0060	0.0065	0.7875	273.193	10.133	0.0454	0.4721
218.156	4.0155	0.0091	0.8242	273.193	12.458	0.0624	0.5242
218.157	4.9846	0.0114	0.8516	273.197	14.867	0.0862	0.5602
218.158	6.0051	0.0140	0.8705				
218.157	7.4985	0.0177	0.8894	280.654 [b]	4.2325	0.0000	0.0000
218.165	9.9819	0.0244	0.9070	280.653	4.4868	0.0020	0.0327
218.166	12.500	0.0298	0.9185	280.654	4.7775	0.0043	0.0676
218.161	14.958	0.0359	0.9255	280.656	5.1334	0.0072	0.1056
				280.655	6.2532	0.0161	0.2016
233.136 [b]	1.0087	0.0000	0.0000	280.657	7.6869	0.0275	0.2872
233.137	1.3855	0.0013	0.2385	280.655	10.079	0.0463	0.3762
233.138	1.7432	0.0026	0.3732	280.657	12.351	0.0662	0.4314
233.139	2.2667	0.0044	0.4967	280.657	14.967	0.0895	0.4708
233.144	3.0449	0.0073	0.6146				
233.146	4.0652	0.0106	0.6922	288.163 [b]	5.0896	0.0000	0.0000
233.150	4.9902	0.0136	0.7363	288.167	5.2805	0.0017	0.0181
233.149	6.1448	0.0173	0.7725	288.162	6.7510	0.0156	0.1303
233.150	7.5195	0.0217	0.8025	288.169	7.7070	0.0245	0.1809
233.149	9.9450	0.0295	0.8351	288.169	9.1920	0.0388	0.2425
233.152	12.342	0.0372	0.8543	288.170	10.234	0.0490	0.2772
233.150	14.868	0.0451	0.8687	288.172	12.843	0.0767	0.3337
				288.169	14.301	0.0938	0.3580
243.093 [b]	1.4280	0.0000	0.0000	288.169	15.089	0.1031	0.3663
243.148	1.8800	0.0017	0.1965				
243.149	2.1307	0.0026	0.2755	295.650 [b]	6.0740	0.0000	0.0000
243.156	3.1976	0.0073	0.4794	295.651	7.4597	0.0163	0.0811
243.156	4.0948	0.0109	0.5713	295.652	9.1282	0.0371	0.1484
243.155	5.0363	0.0146	0.6353	295.652	10.136	0.0507	0.1766
243.159	6.1396	0.0190	0.6840	295.656	12.427 [c]	0.0847	0.2149
243.145	7.5428	0.0245	0.7259	295.660	13.743 [c]	0.1113	0.2170
243.148	10.042	0.0345	0.7712	295.656	13.809 [c]	0.1137	0.2164
243.151	12.343	0.0433	0.7984	295.667	13.879 [c]	0.1157	0.2163
243.150	14.949	0.0531	0.8176	295.667	14.130 [c]	0.1239	0.2143
				295.667	14.277 [c]	0.1290	0.2118
258.060 [b]	2.2909	0.0000	0.0000	295.664	14.414 [c]	0.1346	0.2080
258.146	2.8592	0.0030	0.1474	295.667	14.594 [c]	0.1438	0.2013
258.147	3.2454	0.0050	0.2238	295.666	14.645 [c]	0.1754	0.1993
258.150	4.1368	0.0098	0.3493				
258.151	5.1711	0.0151	0.4453	303.144 [b]	7.2129	0.0000	0.0000
258.151	6.3395	0.0210	0.5171	303.142	7.2801	0.0011	0.0025

258.153	7.5330	0.0272	0.5693	303.144	7.6537	0.0081	0.0149
258.144	9.9881	0.0398	0.6397	303.146	7.7697	0.0104	0.0183
258.147	12.204	0.0508	0.6792	303.145	7.7824	0.0115	0.0191
258.149	15.442	0.0677	0.7145	303.141	7.8040	0.0118	0.0195
				303.144	7.8397	0.0129	0.0202
273.177 [b]	3.4880	0.0000	0.0000	303.149	7.8633	0.0130	0.0208
273.177	4.0825	0.0041	0.0942	303.155	7.9307 [c]	0.0173	0.0227
273.191	4.3654	0.0060	0.1316				

[a] Standard uncertainties are $u(T)$ = 0.005 K, $u(p)$ = 0.003 MPa, $u(x)$ = Max[0.00005, 0.011x(1 - x)], $u(y)$ = Max[0.00005, 0.011y(1 - y)]. [b] CO_2 vapor pressure measurement. [c] Not used in the calculation of the objective function S^2.

Table 6. Coefficients $k_{12,1}$ and $k_{12,2}$ in Eq. (12), values of l_{12}, and objective function S for the binary mixtures studied in this work.

System	Fitted range		$k_{12,1}$	$k_{12,2}$/K	l_{12}	S	Note
	T_{min}/K	T_{max}/K					
$CO_2 + H_2$	218.15	303.15	-1.6748	325	0	0.0084	
	218.15	303.15	-1.8211	300	-0.1157	0.0043	(a)
	218.15	243.15	-1.3917	220	-0.0709	0.0039	
	273.15	303.15	-0.9148	0.0	-0.1119	0.0021	(b)
$CO_2 + N_2$	218.15	303.15	-0.2121	43.0	0	0.0095	
	218.15	303.15	-0.1914	32	-0.0324	0.0076	(a)
	273.15	303.15	0.0112	0	0	0.0013	(b)

[a] recommended parameters.

[b] fit restricted to coexisting states with $x_1 \geq 0.93$

Table 7. Coefficients of Eqs (16) for the near-critical phase envelopes at temperatures T, where p_c is the critical pressure and $x_{1,c}$ is the critical mole fraction of CO_2. [a]

System	T/K	p_c/MPa	$x_{1,c}$	c_1	c_2	c_4	c_5
$CO_2 + H_2$	295.65	14.655	0.8105	1.640×10^{-2}	-1.276×10^{-1}	3.446×10^{-2}	-1.666×10^{-1}
	303.15	7.947	0.9774	-9.411×10^{-3}	-3.502×10^{-4}	-1.131×10^{-2}	-8.109×10^{-3}
$CO_2 + N_2$	288.15	9.968	0.8200	1.120×10^{-1}	-1.692×10^{-1}	-7.339×10^{-3}	-1.417×10^{-1}
	303.15	7.580	0.9864	1.163×10^{-3}	-3.399×10^{-3}	-1.273×10^{-2}	-8.275×10^{-4}

[a] The remaining coefficients are given by $c_3 = (c_1 + c_2)$ and $c_6 = -(x_c + c_4 + c_5)$.

Table 8. Experimental three-phase (S + L + V) locus in the (CO_2 + H_2) and (CO_2 + N_2) systems: temperature *T* and pressure *p*. [a]

T/K	*p*/MPa	*T*/K	*p*/MPa
CO_2 + H_2		CO_2 + N_2	
216.98	4.300	214.87	4.821
217.46	8.881	214.86	4.823
217.94	13.742	213.90	7.842
		212.70	13.018

[a] estimated standard uncertainty of *T* at given *p*, $u(T)$ = 0.1 K.

Table 9. Experimental VLE data for the system CO_2 (1) + N_2 (2) at temperatures T and pressures p, where x denotes mole fraction in the liquid phase, y denotes mole fraction in the gas phase, and u denotes standard uncertainty. [a]

T/K	p/MPa	x_2	y_2	T/K	p/MPa	x_2	y_2
218.147 [b]	0.5601	0.0000	0.0000	258.149	3.3731	0.0197	0.2470
218.157	0.9650	0.0058	0.3845	258.149	4.1673	0.0340	0.3514
218.157	1.5210	0.0138	0.5858	258.149	5.1809	0.0534	0.4272
218.157	2.0400	0.0215	0.6737	258.149	5.9284	0.0688	0.4715
218.157	2.9829	0.0354	0.7538	258.149	7.6148	0.1023	0.5212
218.157	4.0137	0.0512	0.7964	258.149	10.241	0.1716	0.5563
218.157	5.0061	0.0668	0.8177	258.149	12.108	0.2254	0.5343
218.157	6.0019	0.0816	0.8311	258.149	13.245 [c]	0.2842	0.4931
218.157	7.4965	0.1084	0.8373	258.149	13.405 [c]	0.2971	0.4941
218.157	9.9905	0.1450	0.8331	258.149	13.540 [c]	0.3100	0.4793
218.157	12.515	0.1953	0.8151	258.149	13.640 [c]	0.3286	0.3308
218.157	15.028	0.2596	0.7796				
				273.128 [b]	3.4837	0.0000	0.0000
233.151 [b]	1.0093	0.0000	0.0000	273.152	3.5402	0.0011	0.0110
233.152	1.4413	0.0065	0.2578	273.152	4.1499	0.0132	0.1097
233.152	2.0928	0.0166	0.4547	273.152	4.9051	0.0279	0.1931
233.152	3.0096	0.0310	0.5839	273.152	6.5532	0.0622	0.3142
233.152	4.0009	0.0470	0.6585	273.152	8.0680	0.0977	0.3654
233.152	4.9975	0.0637	0.6998	273.152	9.4943	0.1359	0.3849
233.152	6.0123	0.0807	0.7244	273.152	11.031 [c]	0.1943	0.3730
233.152	7.5018	0.1070	0.7427	273.152	11.472 [c]	0.2214	0.3562
233.152	9.9986	0.1544	0.7504	273.152	11.627 [c]	0.2354	0.3464
233.152	12.495	0.2135	0.7403	273.152	11.786 [c]	0.2541	0.3225
233.152	14.963	0.2887	0.6823	273.152	11.792 [c]	0.2495	
243.138 [b]	1.4307	0.0000	0.0000	288.152 [b]	5.0920	0.0000	0.0000
243.151	1.5115	0.0013	0.0439	288.151	5.2408	0.0032	0.0171
243.151	2.0028	0.0097	0.2388	288.151	6.0479	0.0210	0.0897
243.151	3.0074	0.0260	0.4405	288.151	6.8756	0.0403	0.1419
243.151	4.0187	0.0434	0.5419	288.151	8.0236	0.0704	0.1906
243.151	5.0029	0.0616	0.5974	288.151	9.3017 [c]	0.1154	0.2062
243.151	5.9949	0.0806	0.6343	288.151	9.5796 [c]	0.1340	0.1984
243.151	7.6010	0.1121	0.6664	288.151	9.6953 [c]		0.1928
243.151	9.9982	0.1649	0.6766				
243.151	12.561	0.2313	0.6523	303.153 [b]	7.2136	0.0000	0.0000
243.151	14.994	0.3430	0.5706	303.148	7.3072	0.0025	0.0046
243.151	15.207	0.3571		303.148	7.3541	0.0040	0.0068
				303.148	7.4232	0.0063	0.0095
258.144 [b]	2.2925	0.0000	0.0000	303.148	7.5070	0.0099	0.0125
258.149	2.7863	0.0093	0.1360	303.148	7.5717 [c]	0.0122	

[a] Standard uncertainties are $u(T)$ = 0.005 K, $u(p)$ = 0.003 MPa, $u(x)$ = Max[0.00005, 0.011x(1 - x)], $u(y)$ = Max[0.00005, 0.011y(1 - y)]. [b] CO_2 vapor pressure measurement. [c] Not used in the calculation of the objective function S^2.

Table 10. Phase envelopes for the systems CO_2 + H_2 and CO_2 + N_2 interpolated from the experimental data, where p_d is dew pressure, p_b is bubble pressure and T is temperature.

T/K	p_b/MPa	p_d/MPa	p_b/MPa	p_d/MPa
	(0.95 CO_2 + 0.05 H_2)		(0.98 CO_2 + 0.02 H_2)	
273.18	3.78	10.78	3.60	6.42
280.65	4.63	10.53	4.38	6.74
288.16	5.60	10.33	5.28	7.23
295.65	7.34	10.09	6.86	7.77
303.15			7.83	7.95
	(0.95 CO_2 + 0.05 N_2)		(0.98 CO_2 + 0.02 N_2)	
273.13	3.743	5.977	3.580	4.505
288.15	5.557	7.261	5.259	6.009

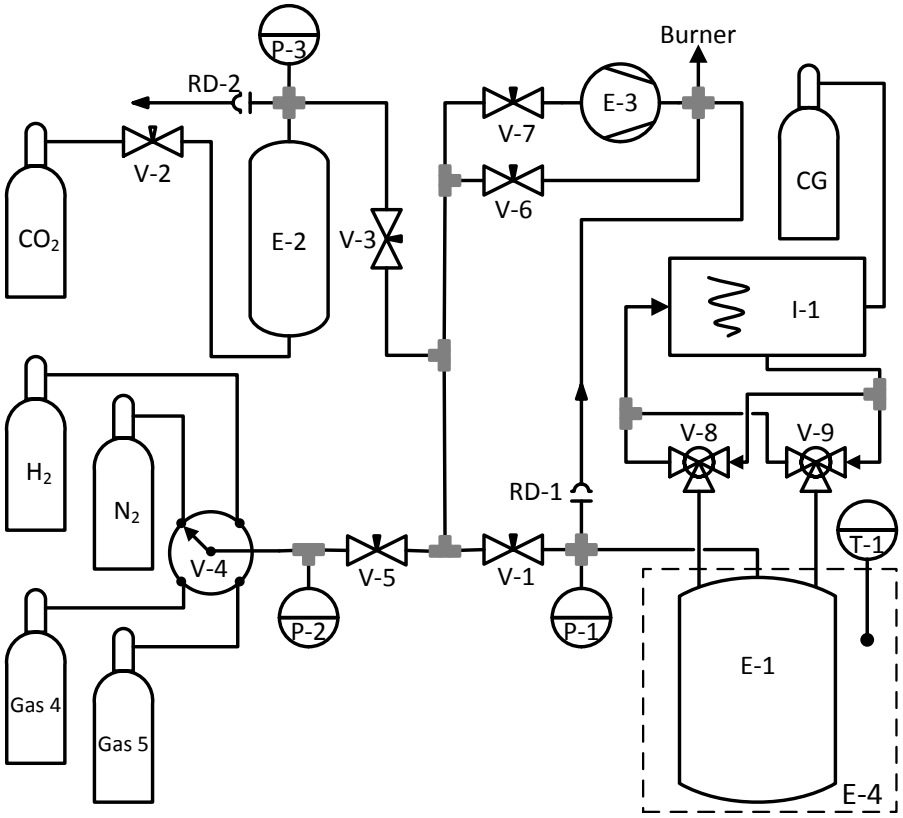

Fig. 1. Simplified schematic of the static-analytic phase equilibrium apparatus: V1 to V3 and V5 to V7, needle valves; V-4, 5-port selector valve; V-8 and V-9, Rolsi sampling valves; P-1 to P-3, pressure sensors; T-1, temperature sensor; E-1, equilibrium vessel; E-2, CO_2 accumulator vessel; E-3, vacuum pump; E-4, thermostatic bath; RD-1 and RD-2, rupture-disc pressure-relief devices; I-1, gas chromatograph; CG, carrier gas bottle.

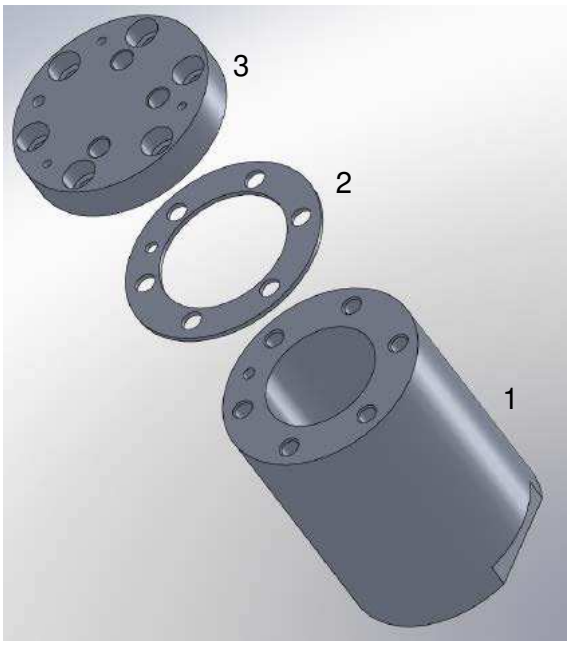

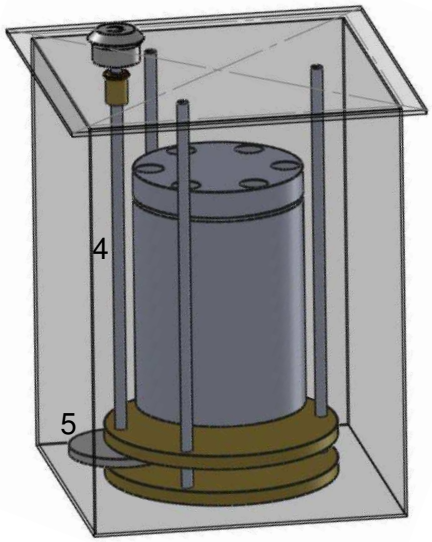

Fig. 2. (a) visualization showing an exploded view of the VLE cell with pot (1), seal retaining ring (2) and lid (3); O-ring and bolts not shown. (b) visualization showing the VLE cell mounted within the bath with stirrer drive shaft (4) and gear/magnet assembly (5).

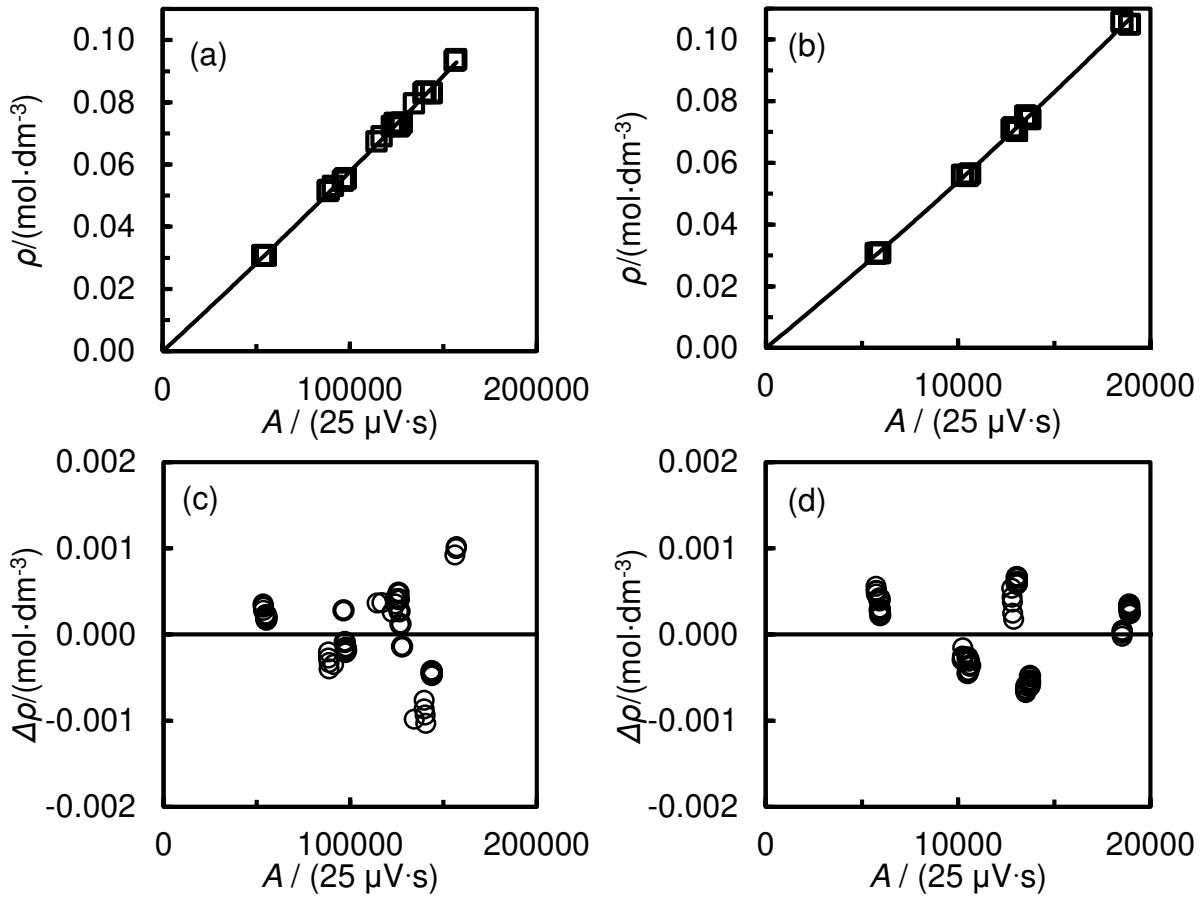

Fig. 3. Thermal-conductivity detector (TCD) calibration data for H_2 (a and c) and CO_2 (b and d) with Ar carrier gas: (a) and (b), gas molar density ρ under filling-loop conditions against area response A; (c) and (d), deviations $\Delta\rho$ of gas molar density from Eq. (1) against area response A. O, experimental data; ——, Eq. (1).

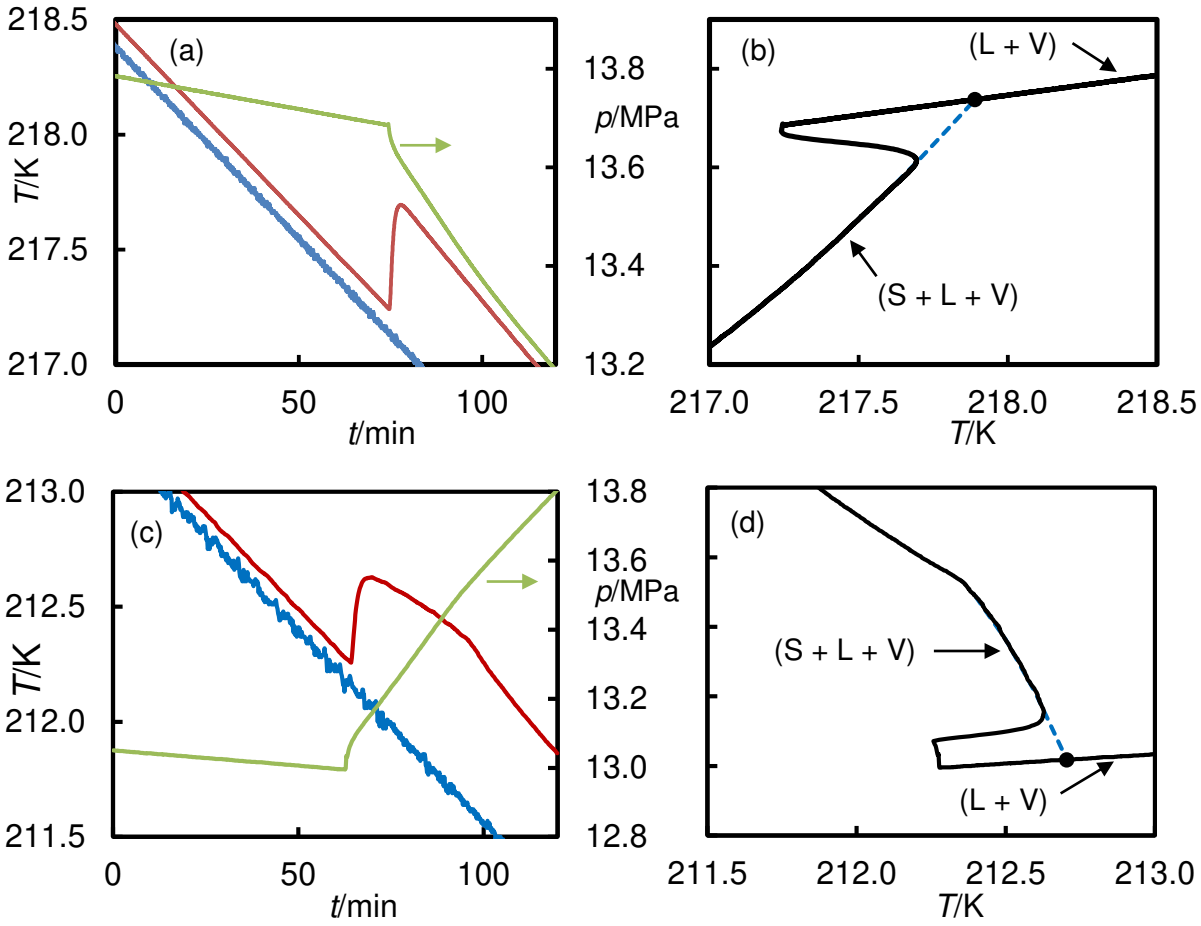

Fig. 4. Cooling ramp in (a and b) (CO_2 + H_2) and (c and d) (CO_2 + N_2). Parts (a and c), temperatures *T* of bath and cell, and pressure *p*, as functions of time *t*. From the bottom: blue, bath temperature; red, cell temperature; green, pressure. Parts (b and d), pressure as a function of cell temperature showing (L + V) branch, supercooled region, and (S + L + V) branch: solid curve, *p*(*T*) along cooling ramp; broken curve, extrapolation of (S + L + V) branch; ●, intersection of (L + V) branch with extrapolated (S + L + V) branch.

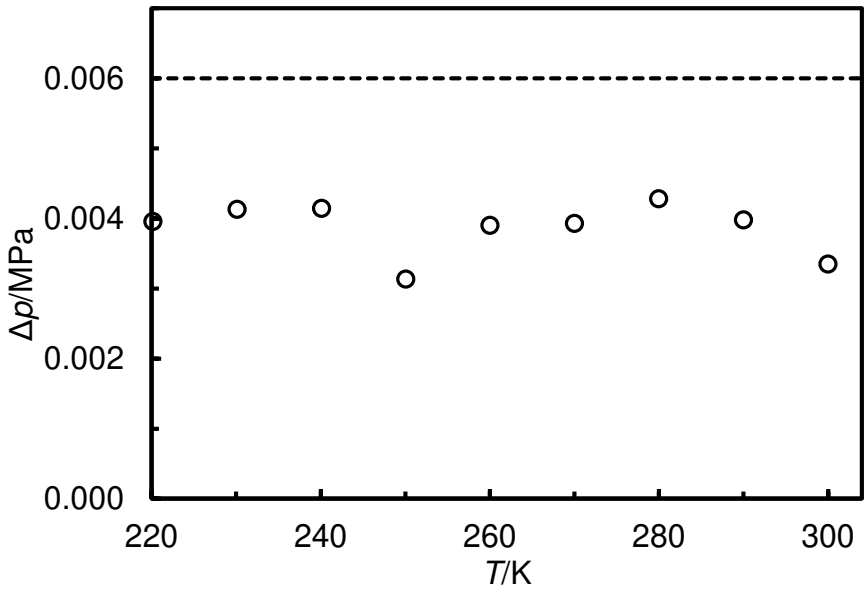

Fig. 5. Deviations $\Delta p = p_{exp} - p_{calc}$ between the experimental vapor pressure p_{exp} of CO_2 and the reference values p_{calc} obtained from the equation of state of Span and Wagner [27] as a function of temperature T: O, this work. The broken line shows the expanded uncertainty of the pressure measurements with a coverage factor of 2.

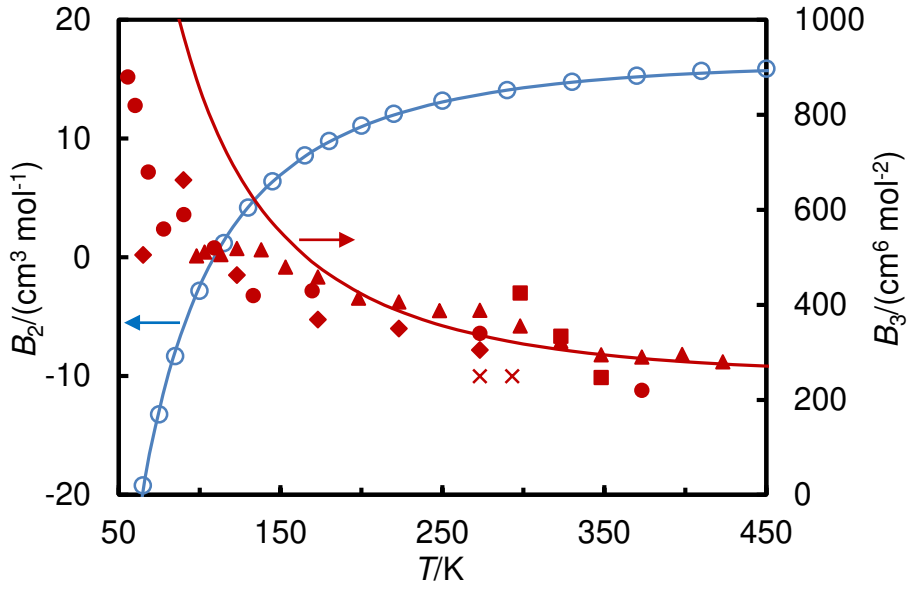

Fig. 6. Second B_2 and third B_3 virial coefficient of H_2. Second virial coefficient: O, recommended by Dymond et al. [30]. Third virial coefficients: ●, Onnes and Braak [31]; ◆,Holborn and Otto [32]; ×, Verschoyle [33]; ▲, Michels et al. [34]; ■; Mihara et al. [35]. Curves are calculated from the Peng-Robinson equation with the effective (fitted) values of T_c, p_c and ω given in Table 4.

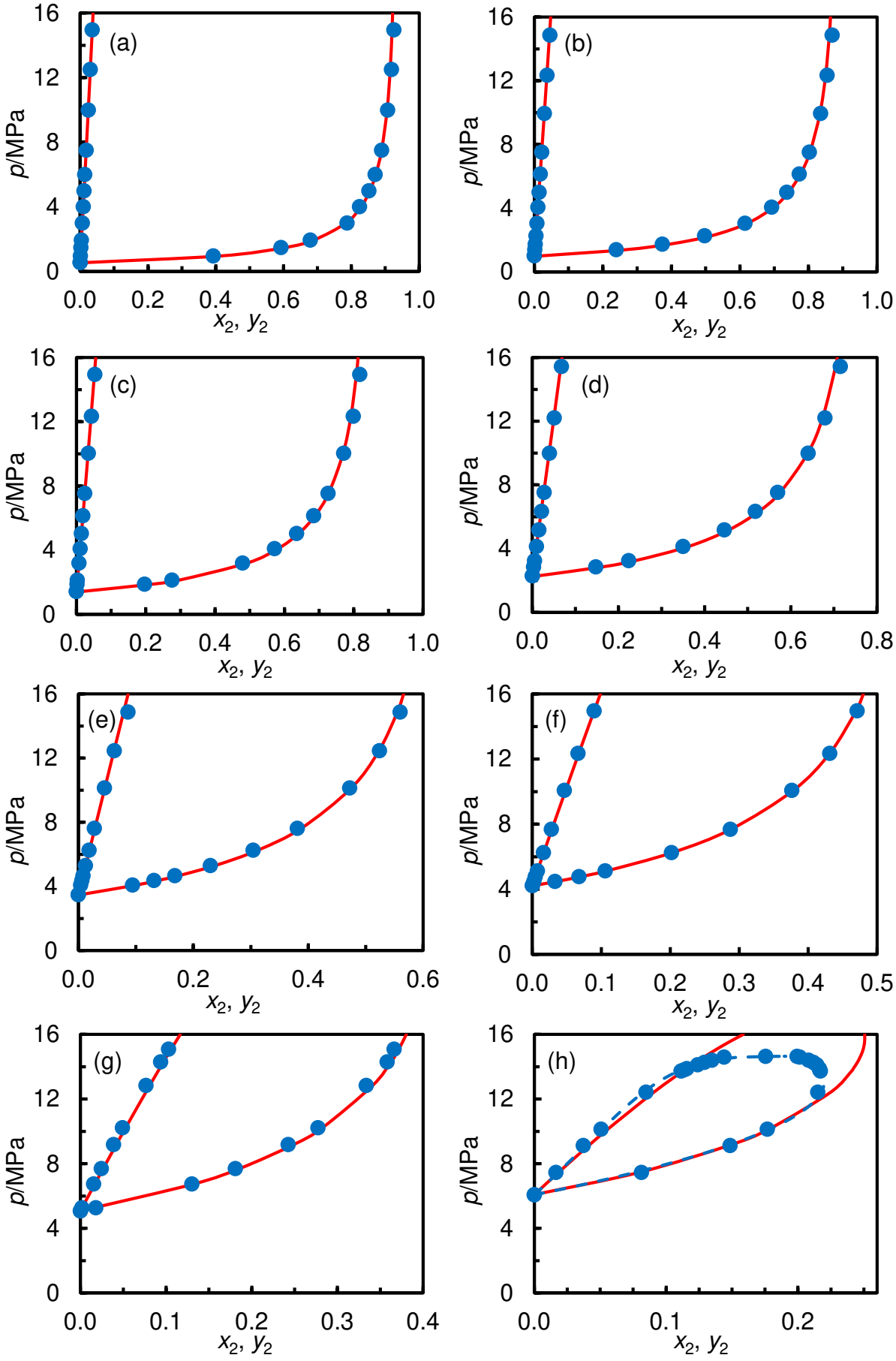

Fig. 7. Pressure-composition diagrams for [CO_2 (1) + H_2 (2)]: ●, this work; ——, Peng-Robinson equation of state with recommended binary parameters from Table 6; – – –, Eq. (16) with parameters from Table 7. (a) T = 218.15 K, (b) T = 233.15 K, (c) T = 243.15 K, (d) T = 258.15 K, (e) T = 273.15 K, (f) T = 280.65 K, (g) T = 288.15 K, (h) T = 295.65 K.

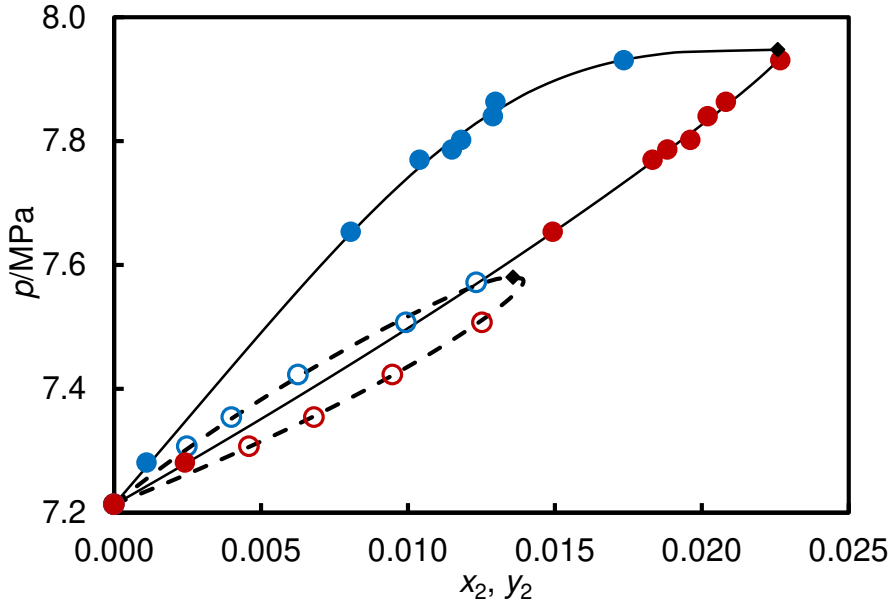

Fig. 8. Pressure-composition diagrams at T = 303.15 K: ●, [CO_2 (1) + H_2 (2)]; O, [CO_2 (1) + N_2 (2)]; ◆, estimated critical point; ——, Eq. (16) for (CO_2 + H_2) with parameters from Table 7; – – –, Eq. (16) for (CO_2 + N_2) with parameters from Table 7.

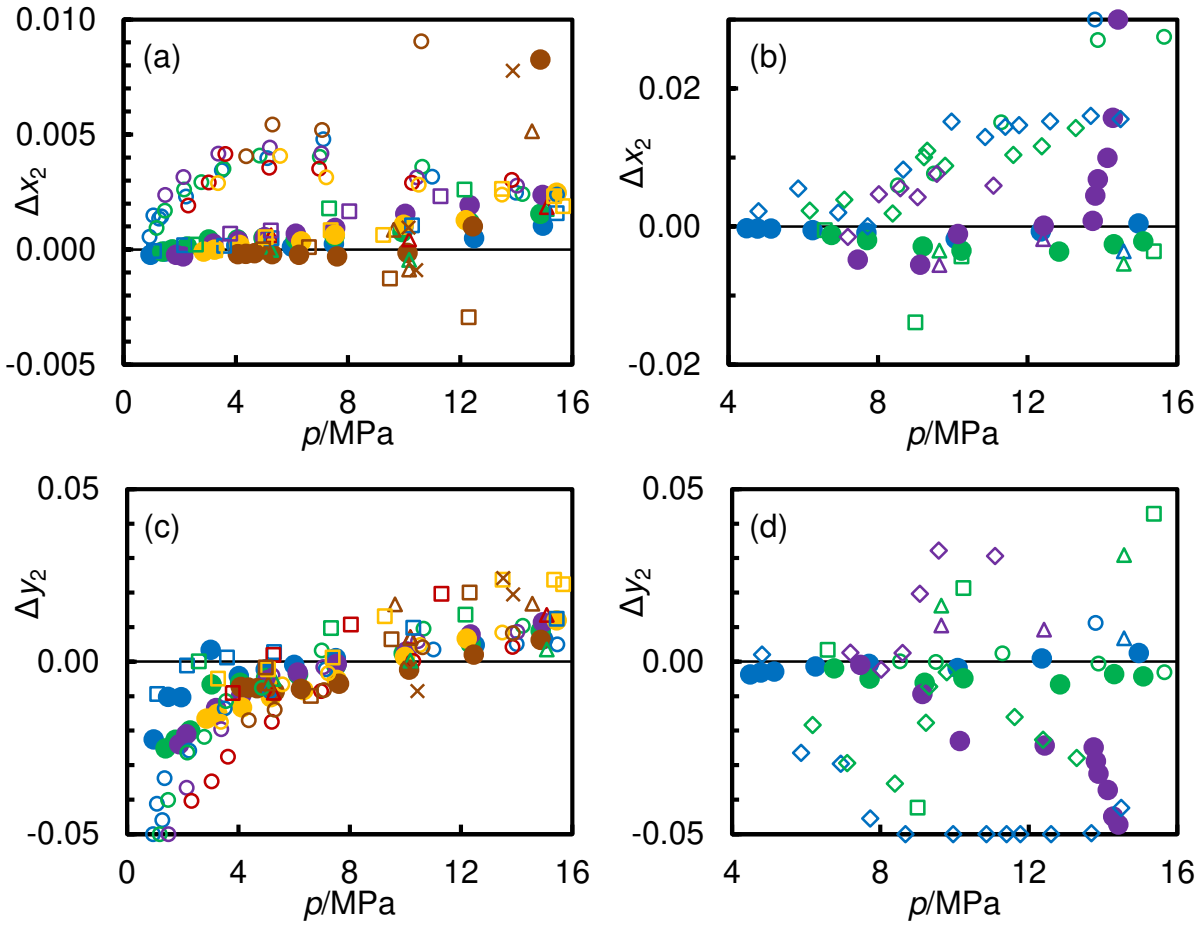

Fig. 9. Deviations $\Delta x_2 = x_{2,exp} - x_{2,calc}$ and $\Delta y_2 = y_{2,exp} - y_{2,calc}$ between experimental mole fractions ($x_{2,exp}$, $y_{2,exp}$) and the values ($x_{2,calc}$, $y_{2,calc}$) calculated from the Peng-Robinson equation of state with recommended binary parameters from Table 7 for [CO_2 (1) + H_2 (2)]: ●, this work, ○, Tsang and Streett [6]; □, Spano et al. [4]; △ Kaminishi and Toriumi [3]; ◇, Bezanehtak et al. [7]; ×, Yorizane [5]. (a) and (c): blue, T/K < 225; green 225 ≤ T/K < 235; purple 235 ≤ T/K < 245; red, 245 ≤ T/K < 255; orange, 255 ≤ T/K < 265; brown, 265 ≤ T/K < 275. (b) and (d): blue, 275 ≤ T/K < 285; green, 285 ≤ T/K < 295; purple, 295 < T/K. Outliers are plotted on the upper or lower horizontal axes.

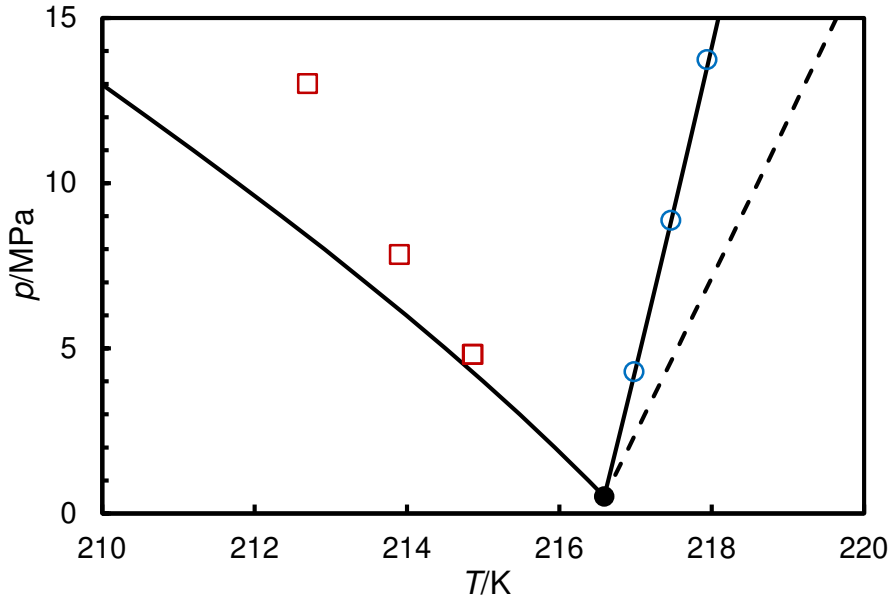

Fig. 10. Three-phase (S + L + V) lines: ○, (CO_2 + H_2); □, (CO_2 + N_2); ●, triple point of pure CO_2; ——, prediction from pure solid + ideal liquid mixture model; – – –, melting line of pure CO_2.

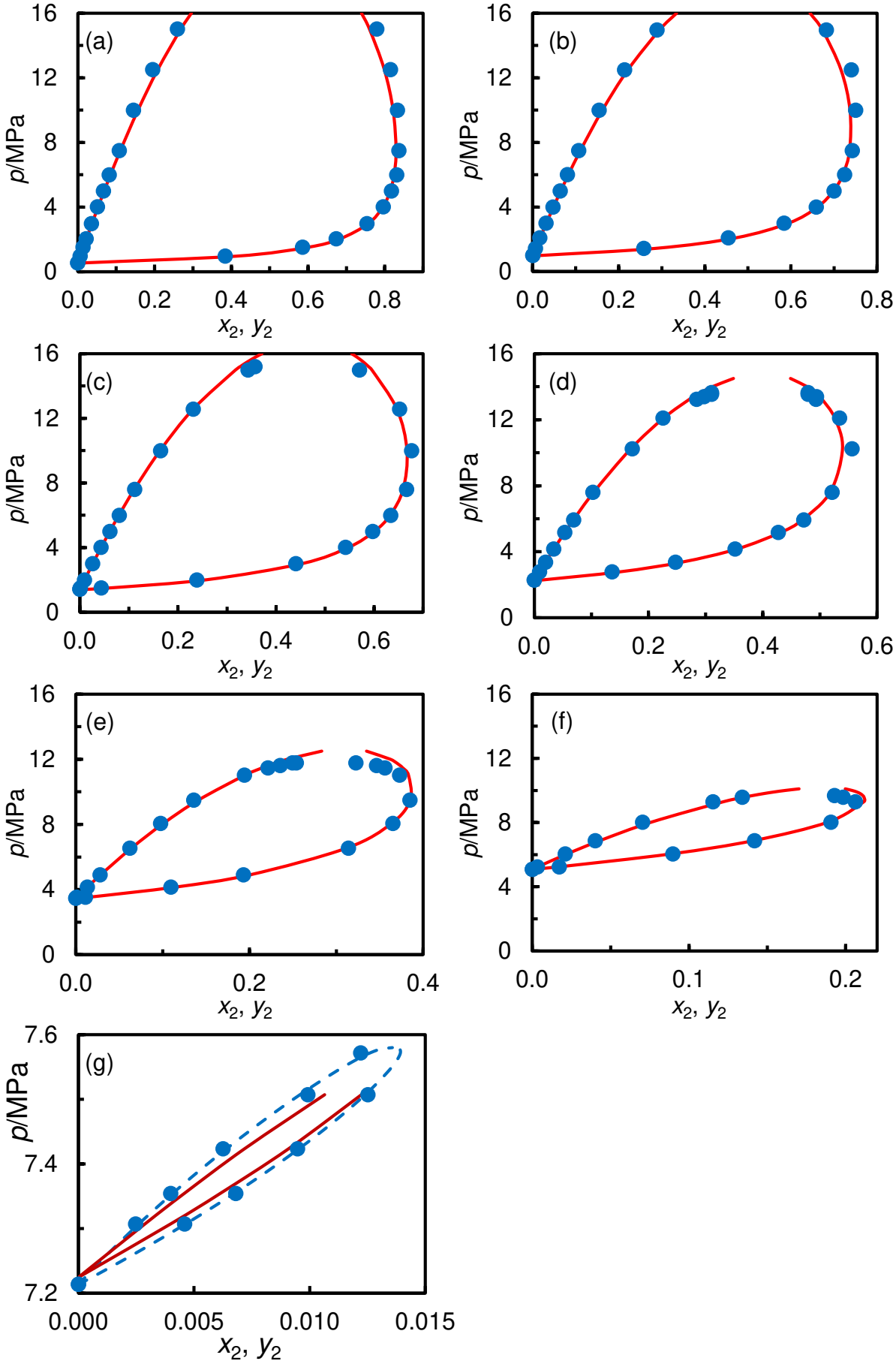

Fig. 11. Pressure-composition diagrams for [CO_2 (1) + N_2 (2)]: ●, this work; ——, Peng-Robinson equation of state with recommended binary parameters from Table 6, – – –, Eq. (16) with parameters from Table 7. (a) T = 218.15 K, (b) T = 233.15 K, (c) T = 243.15 K, (d) T = 258.15 K, (e) T = 273.15 K, (f) T = 288.15 K, (g) T = 303.15 K.

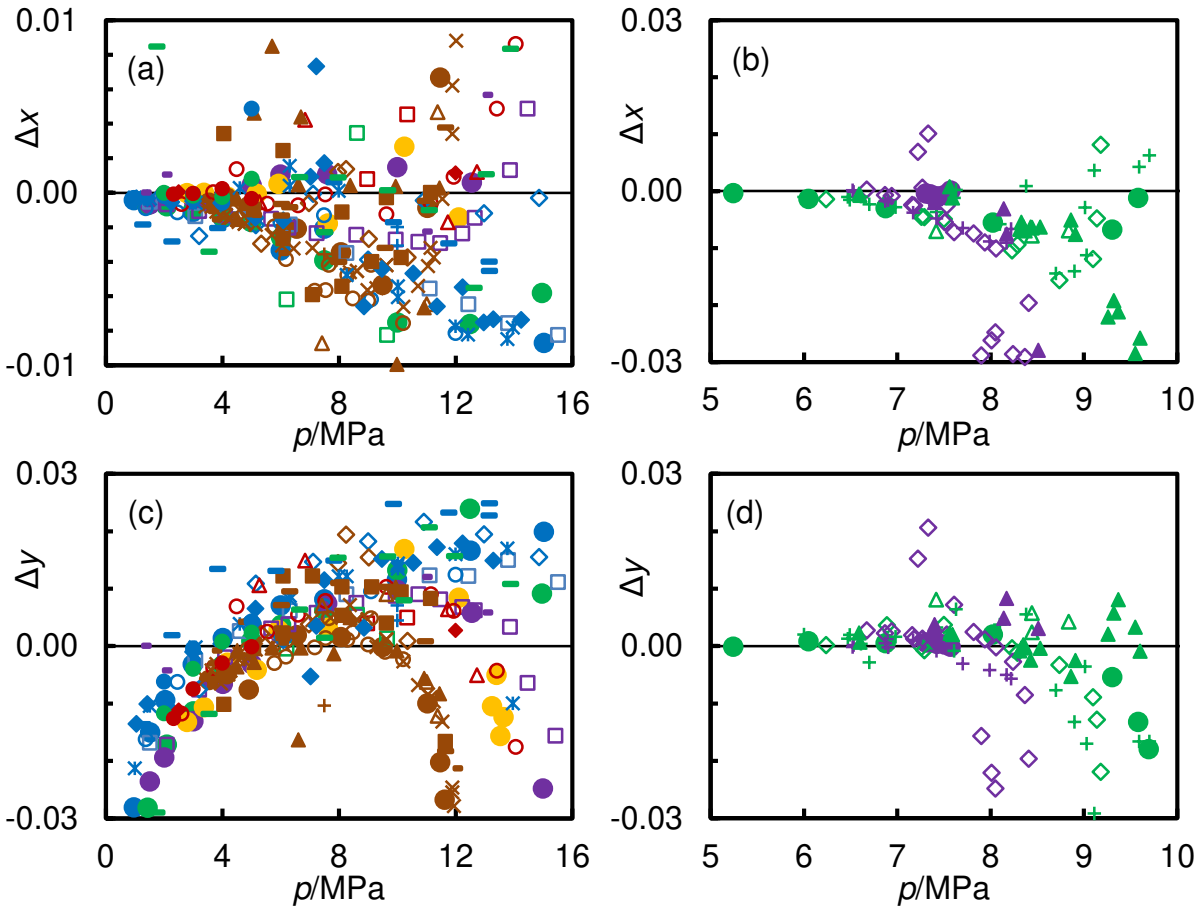

Fig. 12. Deviations $\Delta x_2 = x_{2,exp} - x_{2,calc}$ and $\Delta y_2 = y_{2,exp} - y_{2,calc}$ between experimental mole fractions ($x_{2,exp}$, $y_{2,exp}$) and the values ($x_{2,calc}$, $y_{2,calc}$) calculated from the Peng-Robinson equation of state with recommended binary parameters from Table 6 for [CO_2 (1) + N_2 (2)]: ●, this work, ○, Brown et al. [15, 16, 23]; □, Al-Sahhaf et al. [11]; △ Kaminishi and Toriumi [3]; ◇, Bian and Bian et al. [19, 22]; ×, Somait and Kidnay [39]; ∗, Trappehl [14]; +, Xu et al. [20, 21]; ◆, Yang [18]; ■; Yorizan et al. [5, 10, 13]; ▪, Yucelen and Kidnay [24]; —, Zenner and Dana [9]; •, Zhanzhu et al [25]. (a) and (c): blue, T/K < 225; green 225 ≤ T/K < 235; purple 235 ≤ T/K < 245; red, 245 ≤ T/K < 255; orange, 255 ≤ T/K < 265; brown, 265 ≤ T/K < 275. (b) and (d): blue, 275 ≤ T/K < 285; green, 285 ≤ T/K < 295; purple, 295 < T/K. Outliers are plotted on the upper or lower horizontal axes.

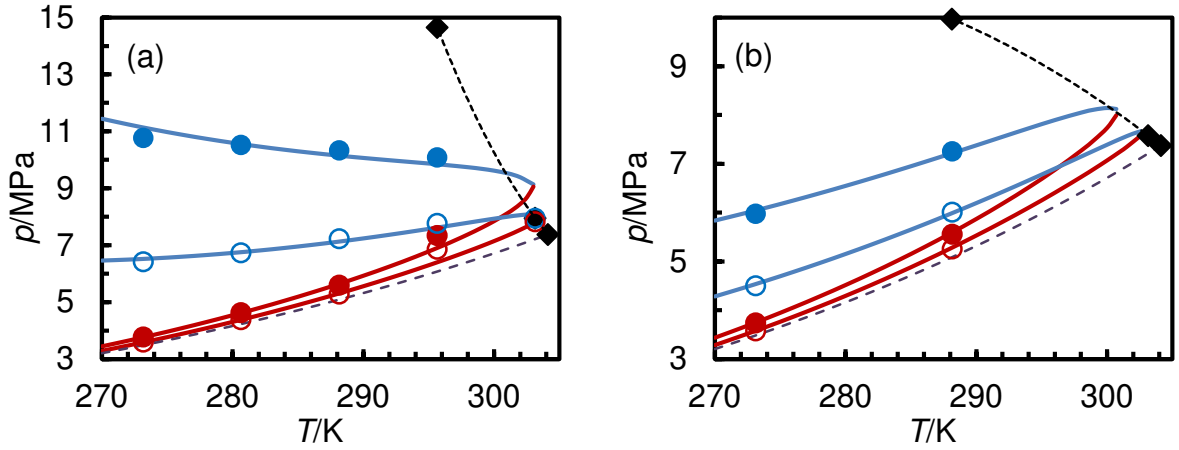

Fig. 13. Pressure-temperature phase envelopes for (a) (H_2 + CO_2) and (b) (N_2 + CO_2): ●, this work interpolated to x_1 = 0.95; O, this work (experimental) interpolated to x_1 = 0.98; ◆, critical points. Solid curves: computed from the Peng-Robinson equation of state with k_{12} = -0.9130 and l_{12} = -0.1147 for (H_2 + CO_2) and k_{12} = 0.0112 and l_{12} = 0 for (N_2 + CO_2). Dashed line: vapour pressure of CO_2. Dotted curves, experimental critical locus. Here, x_1 is the mole fraction of CO_2.

Highlights

- Measurements of vapor-liquid and solid-vapor-liquid equilibria
- Mixtures of CO_2 with H_2 or N_2
- Temperatures from 218 K to 303 K with pressures up to 15 MPa
- Modelling with the Peng-Robinson equation of state
- Applicable to low-temperature CO_2 capture from syngas and pipeline transportation

Graphical abstract